NBS-GCR-88-549

Fractal Analysis of Soot Agglomerates

Roberto J. Samson

June 1988

75 Years Stimulating America's Progress
1913-1988

Sponsored by
U.S. DEPARTMENT OF COMMERCE
National Bureau of Standards
Center for Fire Research
Gaithersburg, MD 20899

NBS-GCR-88-549

FRACTAL ANALYSIS OF SOOT AGGLOMERATES

Roberto J. Samson

University of Maryland
College Park, MD 20742

June 1988

NBS Grant No. COM70NAN850517

Final Report

June 1986 - June 1987

Sponsored by
U.S. DEPARTMENT OF COMMERCE
National Bureau of Standards
Center for Fire Research
Gaithersburg, MD 20899

Notice

This report was prepared for the Center for Fire Research of the National Engineering Laboratory, National Bureau of Standards Under Grant Number COM70NAN850517. The statements and conclusions contained in this report are those of the authors and do not necessarily reflect the views of the National Bureau of Standards or the Center for Fire Research.

The Fractal Analysis of Soot Agglomerates

by
Roberto J. Samson

Thesis submitted to the Faculty of the Graduate School
of the University of Maryland in partial fulfillment
of the requirements for the degree of
Master of Science
1986

ABSTRACT

Title of Thesis : The Fractal Analysis of Soot Agglomerates

Roberto J. Samson: Master of Science, 1986

Thesis directed by: Dr. James W. Gentry
Professor
Department of Chemical and Nuclear Engineering

The fractal behaviour of soot agglomerates formed by the combustion of acetylene in a coannular diffusion burner is studied. Structural data from electron micrographs were obtained by two methods: the first by particle counting with the aid of stereopairs for small clusters, and the second by electronic digitization with advanced image processing techniques, used for the larger agglomerates. An average agglomerate length to width ratio of about 1.7 with a standard deviation of 0.6 was obtained. The agglomerates were found to have a fractal dimension D_f of about 1.8-1.9 based on measurements of the pair correlation function for large agglomerates and 1.5-1.6 based on measurements of the radius of gyration for small agglomerates. These results are compared with recent computer simulations as well as experimental studies of inorganic smokes.

Acknowledgement

The author ackowledges the guidance and support provided by his advisor Dr. James Gentry, and Dr. George Mulholland of the National Bureau of Standard's Center for Fire Research for sharing his expertise on smoke and smoke properties throughout the investigation. Special thanks go to Mr. Eric Steele and Dr. David Bright of the NBS Microanalysis group for the excellent electron microscopy and image processing work provided in this study. Lastly, conversations with Dr. Francis Sullivan of the NBS Scientific Computing Division on the theory of fractals are greatly appreciated.

Table of Contents

page

I. Introduction 1

II. Fractals

A. Background 6

B. Definition of a Fractal 7

C. Agglomerates as Fractals 11

III. Simulations 16

IV. Experimental Procedure

A. Generation of Soot

1. Overview 21

2. Burner Design and Operation 23

B. Soot Characterization 24

C. TEM Image Processing 30

V. Data Analysis 35

A. Particle Counting Method 36

B. Analysis of Large Clusters (5-40 μm)

1. Successive Squares Method 37

2. Pair Correlation Method 38

3. The Sullivan Approach 39

VI. Results 43

VII. Discussion 64

VIII. Recommendations 70

IX. Literature Cited 72

page

VIII. Appendices

A. Successive Squares Method Program 75

B. Pair Correlation Method Program 77

C. Diffusion Limited Aggregation Simulation 80

D. Monte-Carlo Digitization Program 83

List of Figures

page

1. Samples of soot agglomerates formed by acetylene combustion. ... 3

2. A Triadic Koch Curve, $D_f = 1.2618$ 9

3. A Sierpinski Carpet, $D_f \sim 1.89$ 10

4. R_g vs. N plot for Mulholland simulation in the free molecular regime, Ten run average 20

5. Schematic of soot generation apparatus 22

6. Burner schematic showing glass beads location and ceramic honeycomb 25

7. Anderson 2000 cascade impactor diagram 27

8. Size distributions based on aerodynamic diameter for acetylene flows of (a) 42 cm^3/min and (b) 69 cm^3/min 28

9. Digitized micrograph of a cluster consisting of 164 particles, illustrating size parameters L, W, and R_g 32

10. Stereopair of the agglomerate shown in figure 9.......... 33

11. R(size) vs N for experimental data. Cluster sizes defined as R_g or $(LW)^{1/2}$ 45

12. Micrograph and associated c(r) plot for a variety of agglomerate shapes 51

13. Long range effects of shape on c(r) 55

14. Effect of digitizer resolution on c(r) fit for all lines yield slopes $D_f = 1.80 \pm .02$ 59

15. Successive Squares method plot 61

16. Qualitative comparison of clusters produced experimentally and by computer simulations 65

17. R_g vs N plots of experimental and simulation data 66

List of Tables

page

1. Soot production at various flow rates 30

2. Typical results for the particle counting method 44

3. Calculated values of the fractal dimension D_f 49

4. Resolution of mass in digitization process 57

5. Comparison of 3-D and projected D_f values from cluster-cluster agglomeration simulation 63

I. Introduction

Aerosols are suspensions of small particles in air or other gases. Whether formed by the conversion of gases to particulate matter or by the disintegration of liquids and solids, aerosols can have a strong influence on our health and environment. One of the major challenges in aerosol science is to develop an understanding of the relationships between structures and growth mechanisms. In regard to spherical particles, there has been enormous progress in the description of their properties and dynamics. One important aspect of growth is that due to coagulation, which refers to the collision of particles leading to a reduction of the total number concentration. For the special case of droplets, coagulation proceeds by the collision of two particles, which stick together, and finally coalesce [Friedlander,1977].

In the combustion of fossil fuels, ultra-fine soot particles (which are somewhat spherical) are produced from a complex growth process involving nucleation, surface growth (or condensation) and coagulation [Siegla,1981]. These particles may initially fuse upon collision. Eventually, however, the sructural integrity of the particles are maintained, and a cluster made up of these individual primary particles are formed. At the present time, our understanding of the coagulation process resulting in such non-spherical structures is relatively limited. Compared to spherical particles of the same mass, the growth rates of agglomerates will be more rapid due to their greater collision cross-section.

Soot is generated in this manner by automotive engines, industrial processes, and forest fires. An electron micrograph of the soot produced by a laminar diffusion acetylene flame is shown in figure 1. The problem of size classification has often been treated by comparison to the size of a sphere that behaves similarly in regard to a specific property. One example is the use of 'aerodynamic diameters' in impactor measurements to obtain size distributions. Agglomerate 'diameters' based on one property often differ from that based on another. It is therefore evident that a more fundamental description of agglomerate structure is needed.

Recent simulations of particles undergoing Brownian motion with the constraint that the particles stick but do not coalesce upon collision yield clusters that are remarkably similar to actual agglomerates [Meakin,1984]. More importantly, the clusters were described as fractals [Mandelbrot,1977]. That is, a power law relationship between the mass, or number of particles N, and the size of the clusters R (e.g. the radius of gyration R_g), exists in the form

$$N = kR^{D_f} \tag{1}$$

where D_f is the fractal or Hausdorff dimension and k is a proportionality constant. Experimental studies of actual agglomeration processes have also shown similar mass-size relationships. Forrest and Witten [1979] obtained fractal dimensions between 1.5 and 1.7 in their analysis of Fe,

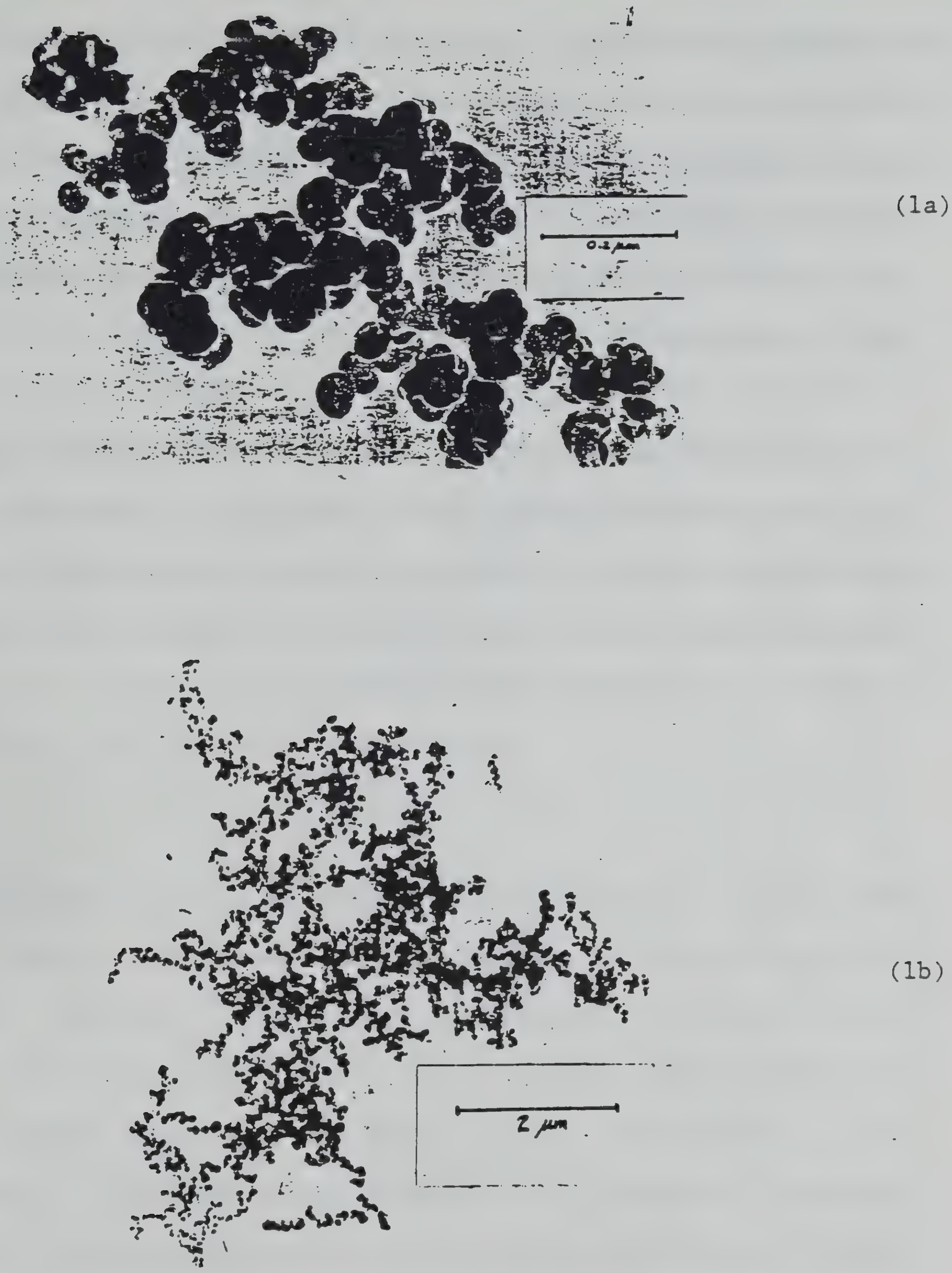

Figure 1. Samples of soot agglomerates formed by acetylene combustion. Magnifications at (a) 100 KX, and (b) 10 KX.

Zn and SiO_2 smokes from transmission electron microscopy (TEM) images. Weitz and Huang [1984] determined gold colloid agglomerates to have a fractal dimension of about 1.70 from TEM and small angle neutron scattering measurements. Feder, et al [1984] reported protein aggregates to have very low sticking probabilities resulting in more compact structures with a dimensionality of about 2.53.

Medalia and Heckmann [1967,1971] characterized primary agglomerates (agglomerates broken down by sonic dispersion) of carbon black in terms of bulkiness, anisometry, and shape factors. The projected area of each agglomerate, A_r, was measured as a function of number of particles N_p. It was determined, for $5 < N_p < 250$ that

$$N_p = (A_r/A_p)^{\alpha} \qquad \alpha = 1.1 \tag{2}$$

where α is the projected area exponent and A_p is the average area of a primary particle in an agglomerate. One cannot infer, however, any fractal behaviour on the basis of their results. In fact, for structures with a fractal dimension less than 2.0 (as suspected for agglomerates), little overlap in mass occurs upon projection, and the cluster is essentially transparent when viewed at any orientation. In the limit of large N_p, the fraction of particles evident upon projection becomes constant. As a result, N_p is directly proportional to A_r, and therefore α has a limiting value of 1.0.

Hence the question of whether this important class of agglomerates exhibited fractal behavior remained to be investigated. This is the motivation of our study, which focuses on soot agglomerates generated in a coannular diffusion burner. We attempt to characterize the structures in terms of the fractal dimension D_f using advanced digitization and processing techniques, on electron micrographs of agglomerates ranging in sizes as little as 50 nm to those as large as 40 μm. The primary objective is to compare experimental and computer modelling results of cluster-cluster agglomeration, as well as similar studies performed on inorganic smokes and gold colloids. Secondly, the effect of cluster shape on the accuracy of the experimental methods and future work involving light scattering (in terms of the pair correlation function) is investigated. It is hoped that the fractal information acquired may in the long run be applied to the study of light scattering and absorption, sedimentation, and diffusion of agglomerates.

II. Fractals

A. Background

In his 1977 essay 'Fractals- Form, Chance, and Dimension', Mandelbrot introduced a new geometry of nature to describe many of the irregular shapes around us which he calls fractals. The most useful fractals involve chance and both their regularities and irregularities are statistical. In addition, the shapes described tend to be scaling, implying that the degree of their irregularities are identical at all length scales. In his analysis, the fractal or Hausdorff [Hausdorff,1919] dimension forms the basis for all subsequent developments.

The formation of clusters by the union of many small elements, termed agglomeration, is an extremely important phenomenon in a variety of processes. These include coagulation in aerosol and colloidal physics, percolation and nucleation in phase transitions and critical phenomena, and gelation and polymerization processes in polymer science, among others. The highly branched and chain-like structure has often been inadequately represented as spherical in accounting for its size in equations of mass and momentum transfer. Witten and Sander [1983], suggested that aggregates of Fe, Zn, and SiO_2 may be classified as fractals. It is only recently that fractal concepts are being applied to other agglomeration processes as well. In the following review of fractals, we shall introduce definitions with the aid of rigid geometric constructs of 1 and 2 dimensional fractals, then lead to the more complex analysis of clusters and random points.

B. Definition of a Fractal

Given a set of points in space, the following relationship holds true if the set is a fractal:

$$K(\underline{a}) = \underline{a}^{-D_f} \tag{3}$$

where D_f is the fractal dimension, and $K(\underline{a})$ is the number of segments (in 1 dimension) necessary to completely 'engulf' or cover the entire set of points. Similarly, $K(\underline{a})$ for a 2 or 3 dimensional set would correspond to the number of circles or spheres, respectively, of radius $\underline{a}$ necessary to cover the set.

In order to understand fully the interpretation of D_f by equation 3, consider the following fractal shapes. Although unrelated to natural systems, they should provide a better understanding of fractal geometries. The first set is a family of 1 dimensional curves Mandelbrot calls a triadic Koch curve, shown in figure 2. The points belonging to the set make up the intervals defined by each straight segment. Figures 2a, 2b, 2c, and 2d have 1, 4, 16, and 48 intervals, respectively. Each succesive shape is generated by replacing the intervals' midthird by the promontary of an equilateral triangle, resulting in a four-fold increase in line segments. The line segments have lengths one-third that of the previous interval. Referring to equation 3, it can be easily shown that the following quantities:

figure 2	(a)	K(a)
a	1	1
b	1/3	4
c	1/9	16
d	1/27	48

lead to a fractal dimension $D_f = (\log 4)/(\log 3) \sim 1.26186$. Note that K(a) tends to infinity as a approaches zero, all within a confined region.

Next we consider a two dimensional Hausdorff set known as a Sierpinski Carpet, illustrated in figure 3. The 'initiator' is a filled-in square (figure 3a), and successive sets are generated by dividing each blackened square into nine equal portions and 'removing' the center square, and so on. K(a) in this set represents the number of squares of side a necessary to cover all of the darkened areas which represent all the points in the set. From the figure, we get

figure 3	(a)	K(a)
a	1	1
b	1/3	8
c	1/9	64
d	1/27	514

and $D_f \sim 1.89$ from equation 3. The Koch curve, Sierpinski carpet, and the other 'designed' fractals described by Mandelbrot all share two important features: the first is their self-similarity, which refers to how a part of the set resembles the whole, and secondly, all obey equation 3, which explicitly describes their scaling behaviour. Note that the self-similarity ratio a was not chosen at will but must be part of a

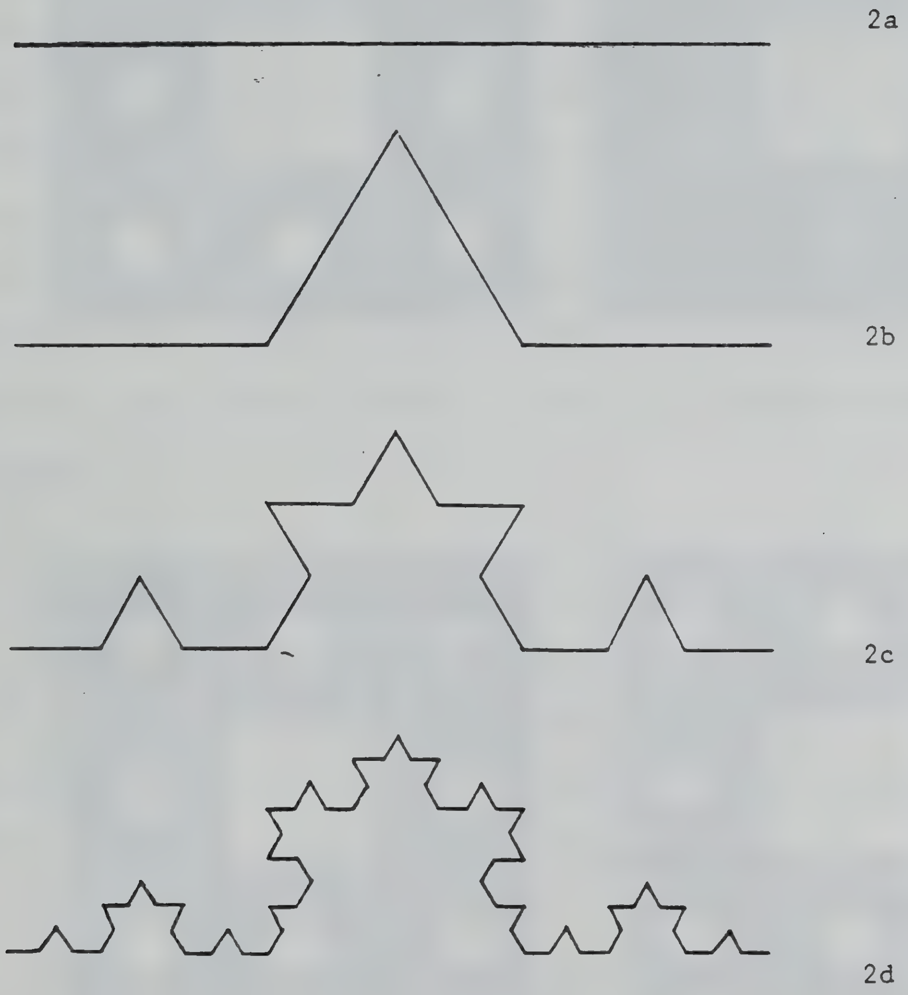

Figure 2. A Triadic Koch Curve, $D_f = 1.2618$. (a) the initiator, and (b)-(d) successive sets generated by replacement of previous intervals' midthird by the promontary of an equilateral triangle. Straight line distance from end points is 1.0.

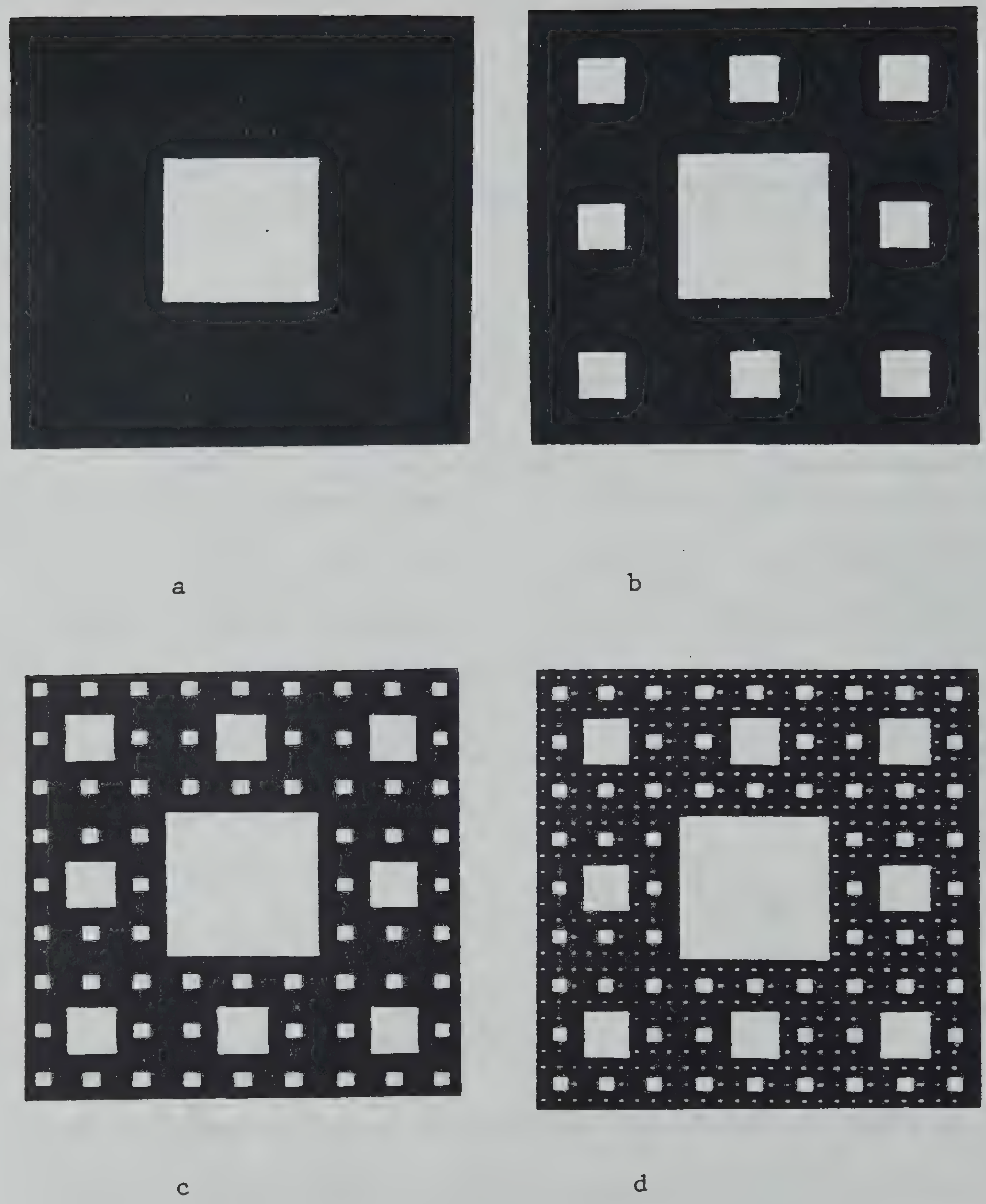

Figure 3. A Sierpinski Carpet, (a) initiator, and (b)-(d) successive sets, $D_f \sim 1.89$.

strict scale, namely 1, 1/8, $(1/8)^2$, and so on.

In contrast, fractals encountered in nature involve a certain degree of randomness. As a result, the self-similarity is less rigid and more statistical. Self-similarity for the case of agglomerates is used in the sense that the relative proportions of the numbers and sizes of void spaces within the agglomerate are identical when viewed at different magnifications. Due to their finite size a limit to this self-similarity is approached when viewed at sizes near that of a primary particle and beyond the overall size of the agglomerate. The following discussion centers on how commonly measurable quantities such as density, number of particles, and radius of gyration can be used in determining the fractal dimension.

C. Agglomerates as Fractals

Suppose we have a 3-D cluster made up of a set of N_T individual particles or 'points'. Recall from equation 3 that $K(\underline{a})$ is the number of spheres of radius a needed to cover the set. The average number of points within each sphere of radius $\underline{a}$ must then be

$$N_{avg}(\underline{a}) = N_T/K(\underline{a}) = N_T \underline{a}^{D_f} \qquad (4)$$

Equation 1 is derived in the following way. Referring to equation 4, it is obvious that as $\underline{a}$ approaches the size of the agglomerate R_g, $K(\underline{a})$ approaches 1, and $N_{avg} \sim N_T$. Therefore

$$N_T \sim R_g^{\,D_f} \qquad (1)$$

as presented.

A new quantity called the pair correlation fuction c(r) is now introduced, and its significance shall be discussed shortly. By definition, c(r) is the average density of points a distance of r from any point. The pair correlation function quantitatively describes the local density fluctuations from the overall density:

$$c(r) = 1/(2\pi rN) \sum_{\mathbf{r}'} < \rho(\mathbf{r}+\mathbf{r}')\rho(\mathbf{r}) > \qquad (5)$$

where <...> represents orientational averaging and $\rho(\mathbf{r})$ is the density at position r, and for TEM images, can be taken as 1.0 at the center of a particle and 0.0 elsewhere. If the set is a fractal, then

$$N_{avg} = \int_0^{\underline{a}} c(r)d^d r \qquad (6)$$

where d is the Euclidean dimension. It follows that an expression for c(r) in the form

$$c(r) \sim r^{\,D_f - d} \qquad (7)$$

for a fractal set satisfies the relationship described by equation 4 when substituted into equation 6. Consider a random distribution of points in d space which has a uniform density. Since the local density is equal to the overall density, D_f=d. Similarly, D_f=d for solid geometric shapes such as spheres and circles.

The pair correlation function has been widely used in the study of fluids and fluid mixtures especially in regard to the fluid properties near the critical point [Kirkwood and Mayer ,1951]. As the critical point of a liquid-vapor system is approached, molecules appear to cluster together in small islands. It was precisely this analogy to agglomeration systems that led Witten and Sander [1981] to believe that computer simulation clusters of diffusion limited aggregation would have similar structural features. In terms of structure at the critical point, the pair correlation function exponent η,

$$c(r) \sim r^{-(d-2+\eta)} \tag{8}$$

is defined. The derivation of equation 8 did not involve fractal theory. Thus for systems at the critical point, the quantity

$$2-\eta \tag{9}$$

plays the role of D_f as shown by equation 8. One must not associate critical point behaviour with the agglomeration process. Of interest is the end result of both processes, and the application of structural analysis techniques (in terms of c(r)) specifically to agglomerates.

The foregoing development of the pair correlation function was presented in light of two main objectives in this study. The first, and most important, is it provides a means of calculating the fractal dimension D_f. Secondly, we wish to validate these findings via light scattering measurements in the near future. It was determined [Stanley,1971] that the intensity of light scattered in the $\mathbf{k}_s$ direction, I(q), can be obtained by taking the fourier transform of c(r):

$$I(q)/I^{\circ}(q) = 1/n \int d(r) e^{-iq.r} c(r) = 1/n\ S(q) \qquad (10)$$

where q = momentum tranfer vector, defined as

$$q = \left| q \right| = 2k\sin(\theta/2) \quad \text{(see following figure)}$$

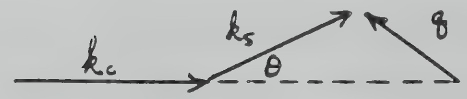

Scattering geometry used to define q [Stanley,1971]

and $I^{\circ}(q)$ = scattering intensity for no particle correlation

$S(q)$ = structure factor, defined as the spatial fourier transform of c(r)

n = number of particles

For isotropic particles, it was shown [Stanley,1971] that

$$I(q)/I^{\circ}(q) = S(q)/n \sim q^{-2+\eta} \qquad (11)$$

provided c(r) is given by equation 8. The relationship between I(q) and c(r) gives an independent method for evaluating D_f. An advantage of light scattering is that the clusters can be studied in a medium where agglomeration is taking place, allowing the analysis of dynamics as well. In addition, the agglomerates are considered as 3-D species as opposed to TEM images where projections of 3-D objects are examined.

From the pair correlation function (equation 7) , the definition of D_f (equation 3), and the mass-size relationship (equation 1), three methods by which D_f can be obtained is now available. In the following section, a review of past and present simulations of agglomeration systems is presented, the results of which will be compared to our experimental data.

III. Simulations

For more than two decades, computer simulations have greatly contributed to our understanding of cluster growth and morphology. In the earliest models of agglomeration, particles were assumed to follow random linear trajectories. A cluster is formed by the addition of single particles in a random manner to a fixed particle located at the center of a square lattice [Vold,1963]. A later treatment included collisions between small clusters as well as primary particles [Sutherland and Goodarz-Nia,1971]. These models, however did not include the Brownian trajectories followed by the particles and clusters. As a result, the important effects which stems from the fact that a random Brownian trajectory has a fractal dimensionality of 2.0 (since it will ultimately cover an entire plane) , while a linear trajectory has a dimensionality of 1.0 were not reproduced by these models [Meakin,1984].

Recently, Witten and Sander [1981] have developed a model that included the addition of single particles following a Brownian trajectory (through random walks) towards a growing cluster fixed at the origin. The resulting clusters exhibited remarkable scaling properties in terms of their growth and internal structure, with a fractal dimensionality of ~ 2.5, but appearing much denser than actual agglomerates.

For purposes of comparison to actual agglomerates, a similar program was created and is listed in appendix C. In this program, an iteration procedure is followed in which an individual particle diffuses a distance of 1.0 lattice spacing from its original position, with the constraint that the particle stick and remain stationary upon contact with the growing cluster (initially a single particle at the origin). After contact, another particle is added at a random point along a radius of $3r_{max}+5$ from the origin, where r_{max} is the distance from the origin to the furthest particle in the cluster. The new particle again diffuses until it collides with the cluster. To decrease execution times, a particle diffusing to a distance greater than $r_{max}+10$ is allowed to travel distances longer than one lattice spacing per move. In addition, particles a distance of $2(r_{max}+5)$ from the origin are considered 'lost' and destroyed, and another one added at the previous starting radius [Meakin,1983].

Although the growth from a single stationary 'seed' seems unrealistic, this model set a precedent for future simulations. Meakin[1984] proposed a more realistic model in which a fixed number of particles, randomly distributed inside a box (cubic lattice), are allowed to diffuse via random walk with the constraint that the particles stick upon collision. This process is termed cluster-cluster agglomeration as opposed to Witten and Sander's diffusion limited aggregation or DLA model which limits diffusion only to individual particles. Periodic boundary conditions are applied to prevent loss of particles through the walls of the box. These simulations, carried out until one cluster remained, resulted in clusters with rather tenuous structures that satisfyingly resemble actual agglomerates, and had fractal dimensions from 1.7-1.9.

More recently, Mountain and Mulholland[1985] applied concepts commonly used in molecular dynamics to the problem of cluster-cluster agglomeration. In lieu of the previous Monte-Carlo techniques, the particles and clusters rigidly diffused according to the Brownian motion rule governed by the Langevin equation (in 1 dimension):

$$d(mv_x)/dt = - m\beta v_x + f_x \tag{12}$$

where m is the mass of the agglomerate, β the aerosol relaxation time and f_x a stochastic force. The quantity v_x is the velocity in the x direction defined as

$$dx/dt = v_x \tag{13}$$

This allowed the history of the growth process to be studied in detail by straightforward comparison of the kinetics of a real system. Derived expressions for β allowed simulation in both the free molecular and continuum regimes. The solution to (14) assumes the particles are in thermal equilibrium with the background gas:

$$r = r_0 + 1/ \beta(v+v_0)\tanh(\beta h/2) + B_2 \tag{14}$$

$$v = v_o e^{-\beta h} + B_1 \tag{15}$$

where r and v are the positions and velocities at time t+h, given r_o and v_o for time t. B_1 and B_2 are stochastic integrals satisfying

$$<B_1> = <B_2> = <B_1 . B_2> = 0 \qquad (16)$$

$$<B_1{}^2> = 3k_B T/m[1-2\tanh(-2\beta h) \qquad (17)$$

$$<B_2{}^2> = 6k_B T/m\beta^2[\beta h-2\tanh(\beta h/2)] \qquad (18)$$

where k_B is Boltzmann's constant and T is the absolute temperature. The reader is asked to refer to a paper [Mountain and Mulholland,1985] for a detailed discussion of the simulation beyond the scope of this report.

Plots of $\log(R_g)$ versus log(k=number of particles) yielding D_f values between 1.70 and 1.90 were obtained. Figure 4 is one such plot averaged over two simulations in the free molecular regime for $\beta\tau = 0.05$ (τ is the time required to free stream a particle diameter, set = 1.0) and density = .0167. Greater scatter for large R_g is observed due to an inherently smaller number of the large relative to the small agglomerates produced. These results (in terms of D_f) agree quite well with Meakin's Monte-Carlo simulation.

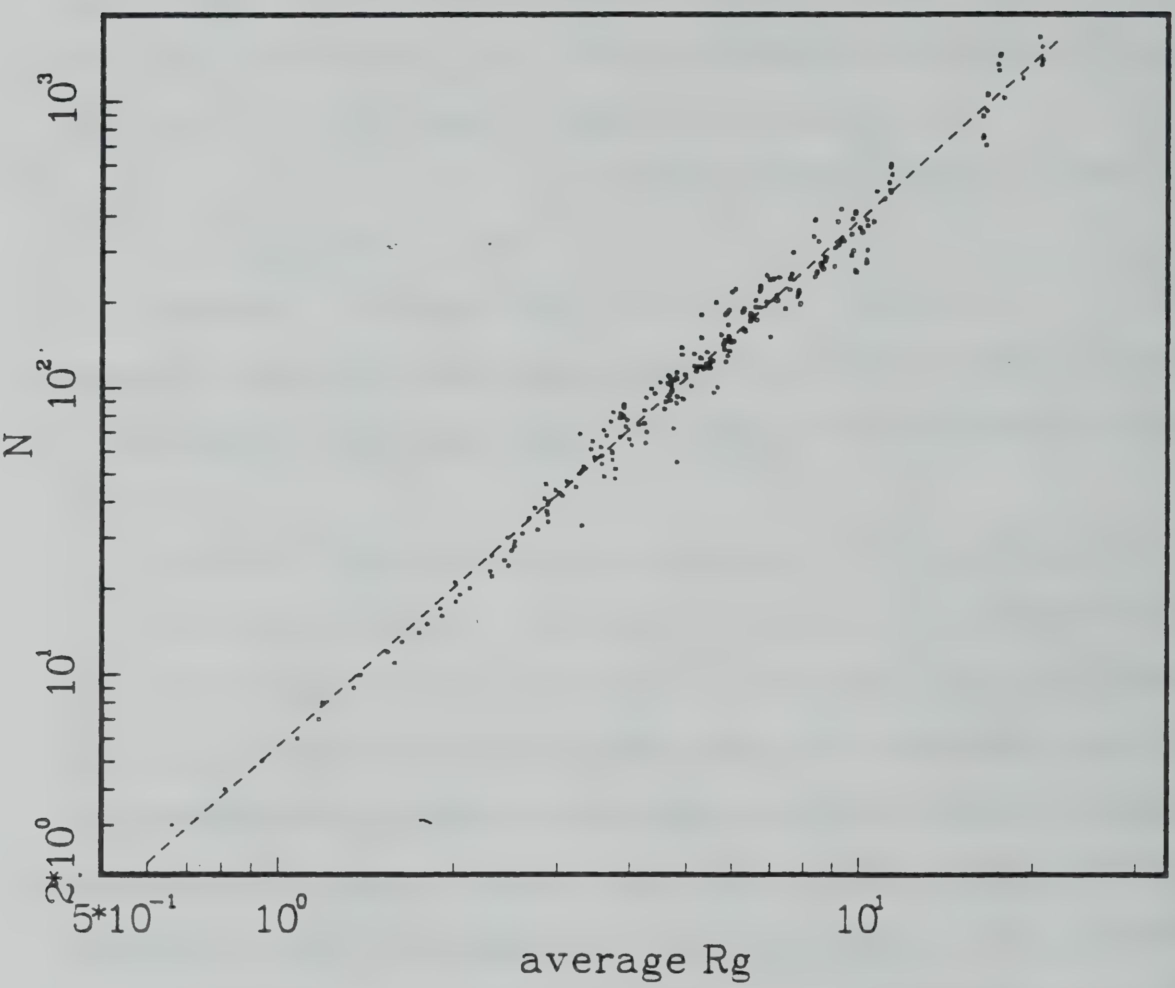

Figure 4. R_g vs. N plot for Mulholland simulation in the free molecular regime, five run average.

IV. Experimental Procedure

A. Generation of Soot

1. Overview

Figure 5 shows the apparatus used to produced the soot agglomerates. The three principal components of the system are:

(1) a coannular diffusion burner,
(2) a glass chimney and dilution chamber, and
(3) flow controllers.

The burner design is similar to that used by Santoro[1983] to obtain particle concentration profiles within the flame. Acetylene (99.9%), is chosen as the fuel source due to its high sooting tendencies. The fuel flows through a 1.27 cm (1/2 inch) nominal brass tube at the center of the burner. Air is introduced through two inlet ports at the bottom at a rate of 40 l/min and flows laminarly and uniformly across the top. Pre-mixing of air and fuel is not allowed prior to combustion (diffusion flame). Once the proper air and fuel flow rates have been selected, the fuel is ignited, and a glass chimney is placed over the burner. A fine thread of smoke emerges from the laminar flame which extends to a height 30-35 cm from the base of the flame. At this height some back-mixing occurs due to the flow constriction at the top, as evidenced by the dispersion of the fine thread of smoke in this area. Agglomeration begins in the flame and proceeds as the clusters traverse the length of the thread. Large agglomerates, in the order of about .2-.5 mm, precipi-

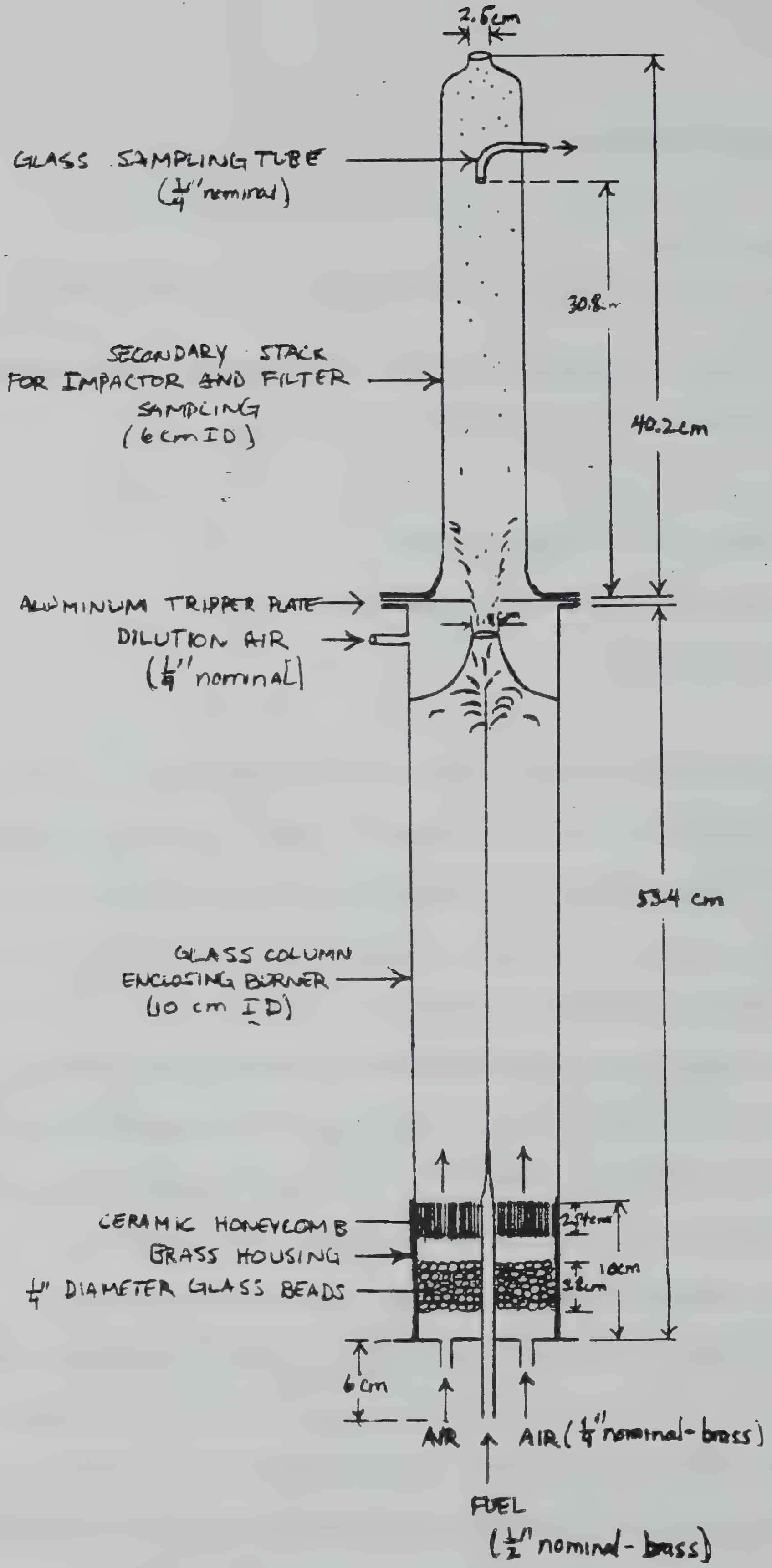

Figure 5. Schematic of soot generation apparatus.

tate out of the region below the funneled top at high fuel flow rates, suggesting that agglomeration occurs to some degree by backmixing. The species are sampled by briefly passing TEM carbon coated grids (3 mm diameter, .13 mm thick, and 200 mesh copper) over the top of the column. We believe that the agglomerates are drawn towards the grids by themophoresis [Davies,1966] as opposed to impaction or diffusion. The relatively weak dependence of thermophoresis on particle size allows size ranges between three orders of magnitude to be collected [Hinds,1982]. Samples were collected only for a short period of time to avoid impaction of clusters on top of one another on the TEM grid. A previous study [Weitz and Huang,1984] of gold colloid agglomerates produced in aqueous solution indicated a flattening and hence distortion of the clusters on the TEM grid during the sample drying/preparation process. In our investigation, these procedures were not required prior to TEM analysis. Thus the 3-D structural features are preserved, as later seen upon examination of the clusters from different viewing angles.

2. Burner Design and Operation

A schematic of the coannular diffusion burner is given in figure 6. The design specifications require that the flow of acetylene should be laminar and variable between 40 and 150 cm^3/min. To insure this a 1/2" nominal brass tube (pure copper is reactive to acetylene) is used, limiting the Reynolds number to < 10.0 at the maximum flow of 150 cm^3/min. A tube length of 16 cm eliminates possible entrance effects and assures fully developed flow (length $> .04$ Re).

In order to maintain a stable flame, assure a sufficient supply of oxygen for combustion, and to confine the smoke produced into a finer thread above the flame, a laminar stream of air flows vertically through the top of the burner. As noted earlier, air is introduced at the bottom through two inlet ports. The air is dispersed uniformly inside the burner as it flows through three chambers, essentially composed of 2 empty chambers between two meshed screens a distance of 3.8 cm apart, packed with 1/4 in.(.64 cm) diameter glass beads. Laminar flow is achieved by passage through a 1 in. thich ceramic honeycomb with 1 mm vertical channels. As also mentioned, a glass chimney with a height of 53 cm (about .3 cm thick) encloses the entire burner from its base to about 40 cm above it. This proved to be crucial in preventing external air currents caused by laboratory exhausts from distorting the steady flame and soot path. In addition, the funnel shaped top provides an area of greater soot concentration suitable for sampling. The stack was constructed of glass to allow the operator to visually monitor flame and sooting conditions.

B. Soot Characterization

Cascade impactor and sooting efficiency measurements are taken by sampling a fraction of a cross-sectional path followed by the aerosol. The soot concentration must therefore be uniform across the sampling area. To meet this criteria, the gas and particle mixture exiting the chimney is diluted with an additional 30 liters/min of air and is dispersed through a 1 inch hole centered on a rectangular aluminum tripper plate. A second stack (mixing chamber) placed directly on the

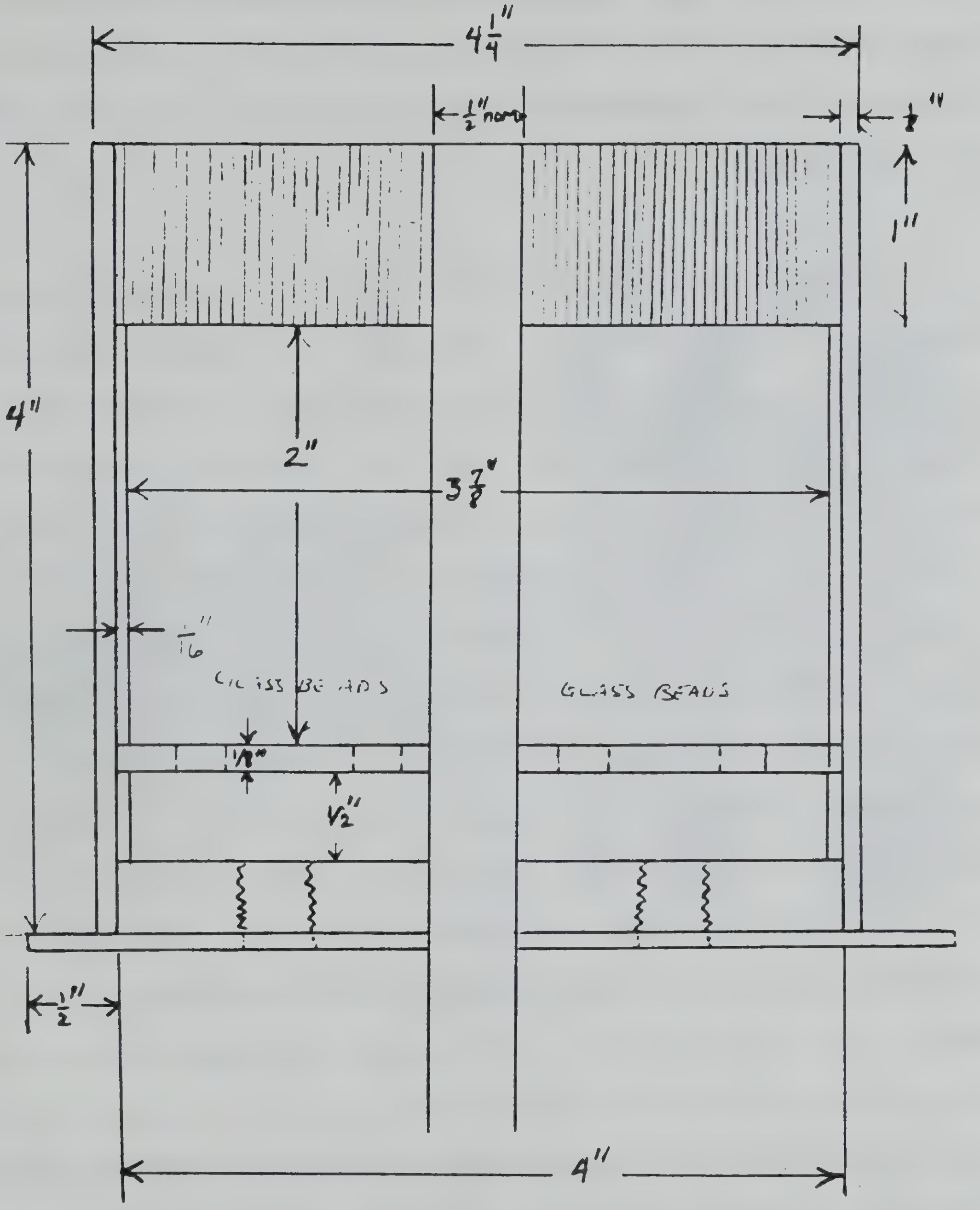

Figure 6. Burner schematic showing glass beads location and ceramic honeycomb. Plate at base of burner supports glass chimney.

plate provides a path where turbulent flow is allowed to develop, and a .64 cm (1/4 inch) glass tube situated at the center of the stack 30.8 cm above the plate is used for sampling. We note that once the soot is dispersed, futher agglomeration is unlikely because of increased inter-particle distances.

Size distributions for two flow rates were determined using an Anderson 2000 cascade impactor. The impactor is comprised of eight stages, each consisting of an aluminum orificice plate and a base for filter support (figure 7). The stages are sealed with O-rings and held together by three spring clamps. Orifice diameters are the same on each plate, but get increasingly smaller in each succeeding stage. When air is drawn through the sample, impaction on any given stage depends on the particle aerodynamic diameter, defined as the diameter of a hypothetical sphere of unit density with the same Stokes number (or settling velocity) as the particle in question [Friedlander,1977]. The jet velocity of the stage and the cut-off of the previous stage determines the range of particle sizes collected on each stage. Particles not collected on one stage follows the gas stream around the edge of the plate to the next stage, where it is impacted or passed to the next, until the jet velocity is sufficient for impaction. The air from the burner is sampled at 1.0 cfm for a pre-determined period, depending on particulate concentration. At this flow the particulate fractionation range is limited from .4 to 10 μm diameter. Figure 8a and 8b are size distributions at fuel flows of 42 and 69 cm^3/min, respectively. The average diameter is shown to increase by a factor of ten between the two

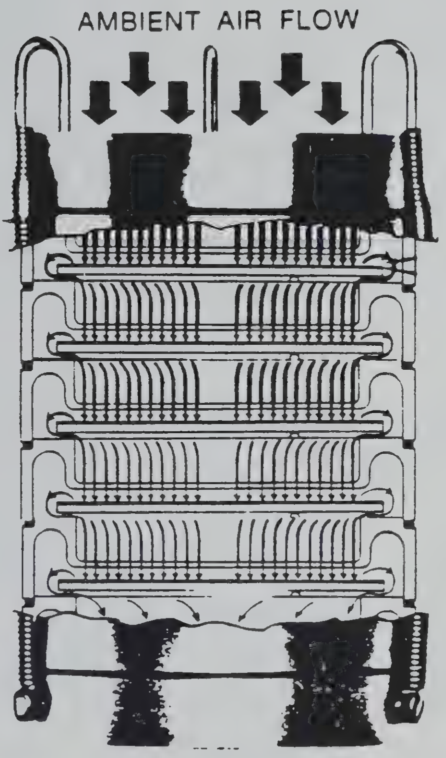

SCHEMATIC CROSS SECTION OF THE NON VIABLE IMPACTION STAGES. PROGRESSIVELY SMALLER ORIFICES INCREASE THE ORIFICE VELOCITY IN EIGHT SUCCESSIVE STAGES CAUSING IMPACTION OF SMALLER PARTICLES ONTO THE COLLECTION DISCS OF EACH SUCCEEDING STAGE.

Figure 7. Andersen 2000 cascade impactor diagram [Andersen,1977].

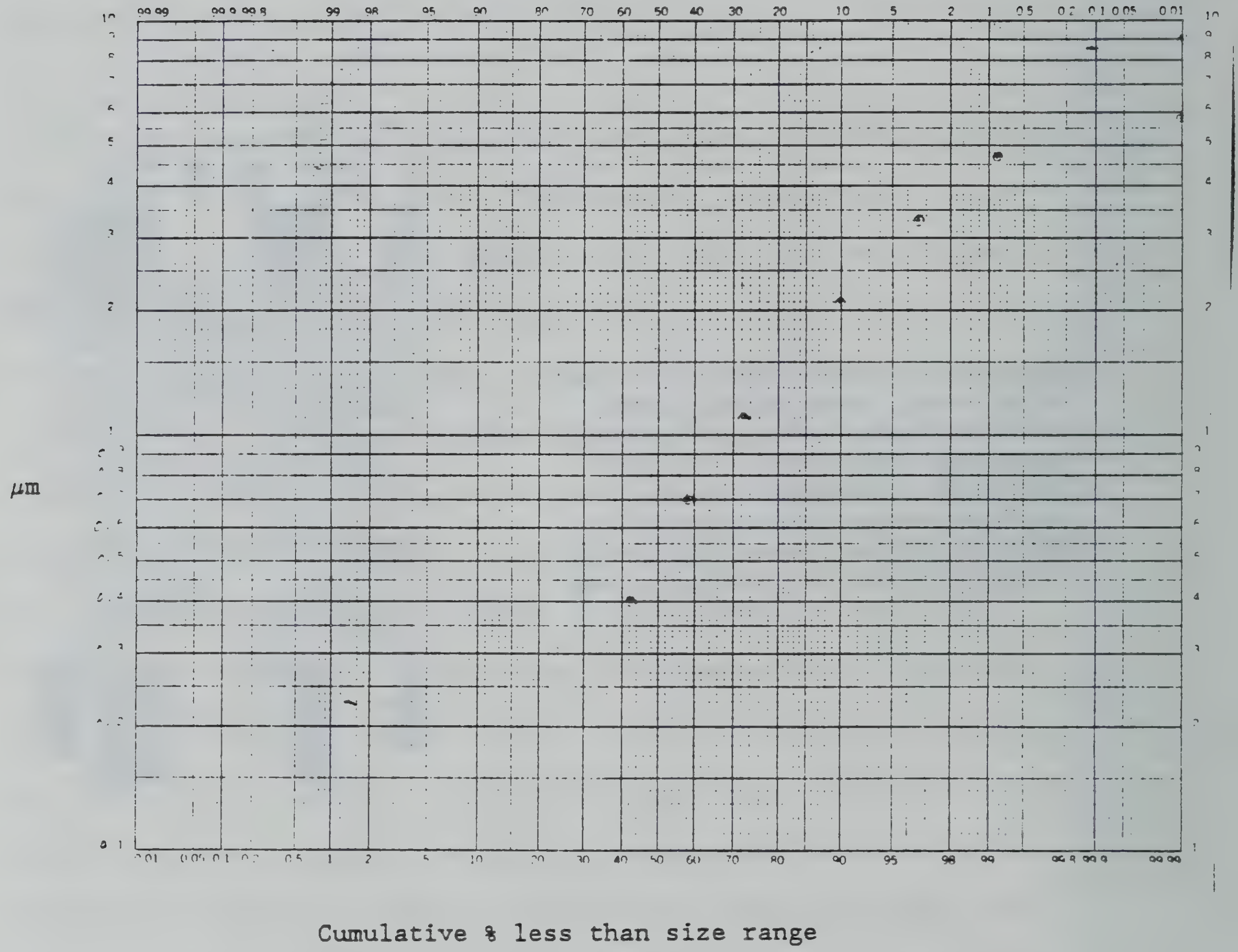

Figure 8a. Size distributions based on aerodynamic diameter from impactor measurements at fuel flow of 42 cm^3/min.

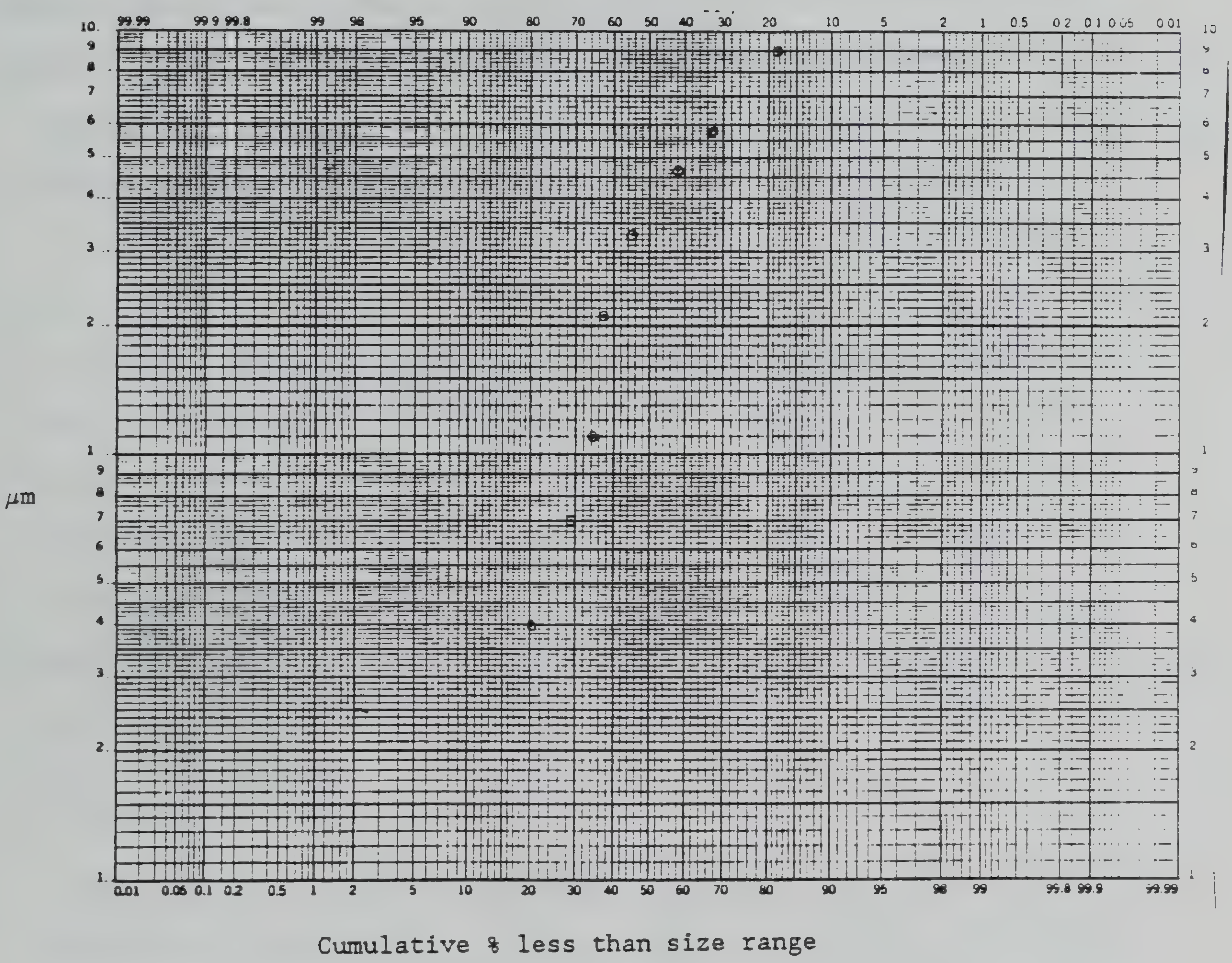

Figure 8b. Size distributions based on aerodynamic diameter from impactor measurements at fuel flow of 69 cm^3/min.

flow rates, from .48 to 5.8 μm.

The flows of air and fuel must be steady to insure consistent measurements. Air flows are controlled by Tylan FC 261 and 262 mass flow meters that adequately compensate for line pressure changes. A Matheson 602 ball meter (calibrated with a bubble meter) was used to vary fuel flow. Table 1 is a list of sooting efficiencies at different flow rates.

Acetylene Flow (cm^3/s)	mg soot produced per mg C_2H_2 burned
0.92	.0445
1.16	.0639
1.46	.0671
1.78	.0699

Table 1. Soot production at various flow rates.

Samples ranging from 0.1 to 1 μm were determined to be best obtained at a fuel flow rate of ~ 1.0 cm^3/s . Larger agglomerates (5-38 μm) were sampled at a rate of ~ 1.5 cm^3/s. Prior to TEM analysis, preliminary specimens where collected on microscope cover slips for viewing on a 90X objective lens to determine appropriate flow conditions. TEM micrograph digitization procedures will now be discussed.

C. TEM Image Processing

The TEM images can be classified into two cluster size categories. The first category make up clusters about 200 primary particles or less, to be used in the 'particle counting' method. Magnifications in this category ranged from 73 to 330 KX, depending upon cluster size and image resolution. In this method, the micrographs were enlarged to 8 x 10 photographs, and the center of each primary particle recorded on an Hewlett Packard 87 with a digitizing tablet. Figure 9 is one such image. To aid in distinguishing overlapping particles, stereoscopic pairs of the images were also used. To create a stereoscopic pair, two electron micrographs of the same cluster are made, with the second image taken after the sample is rotated approximately 10° from the axis of tilt. The Jeol 200cx transmission electron microscope has a viewing stage that is capable of tilting the TEM grid (and thus the sample) by 30° in either direction. When viewed side by side through special lenses, one is able to perceive three dimensional features of the cluster. An example of a stereopair is shown in figure 10. Gray, et al[1985] found that the number of particles counted in large samples of diesel particles was about 36% greater using stereoscopic pairs as opposed to conventional viewing of 2-D images.

Agglomerates between 5 and 40 μm constitute our second size category. In this set, each micrograph is converted to an electronic grid of 512 x 512 pixels. Each pixel, as viewed on a high resolution monitor, has an associated gray level which can have values from 0 to 255. A gray level of 0 signifies the lightest gray, while 255 the darkest gray level. Using an image processing program known as Lispix, appropriate gray level 'thresholds' are chosen to determine which pixels represent areas on the grid that are occupied by a particle. For example, if a digitized image

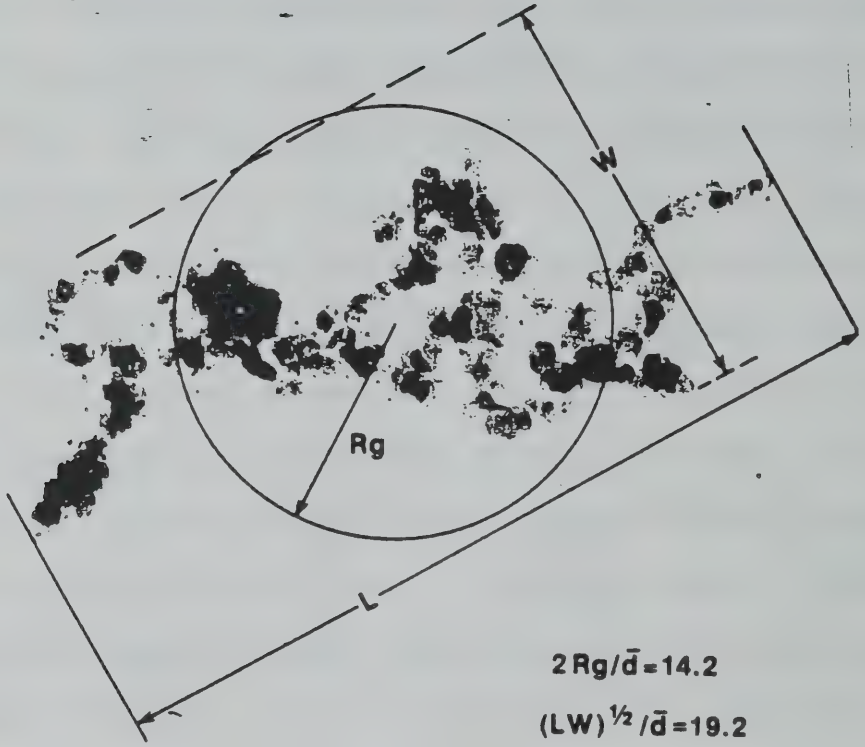

AGGLOMERATE SIZE PARAMETERS

Figure 9. Digitized micrograph of a cluster consisting of 164 particles, illustrating size parameters L, W, and R_g.

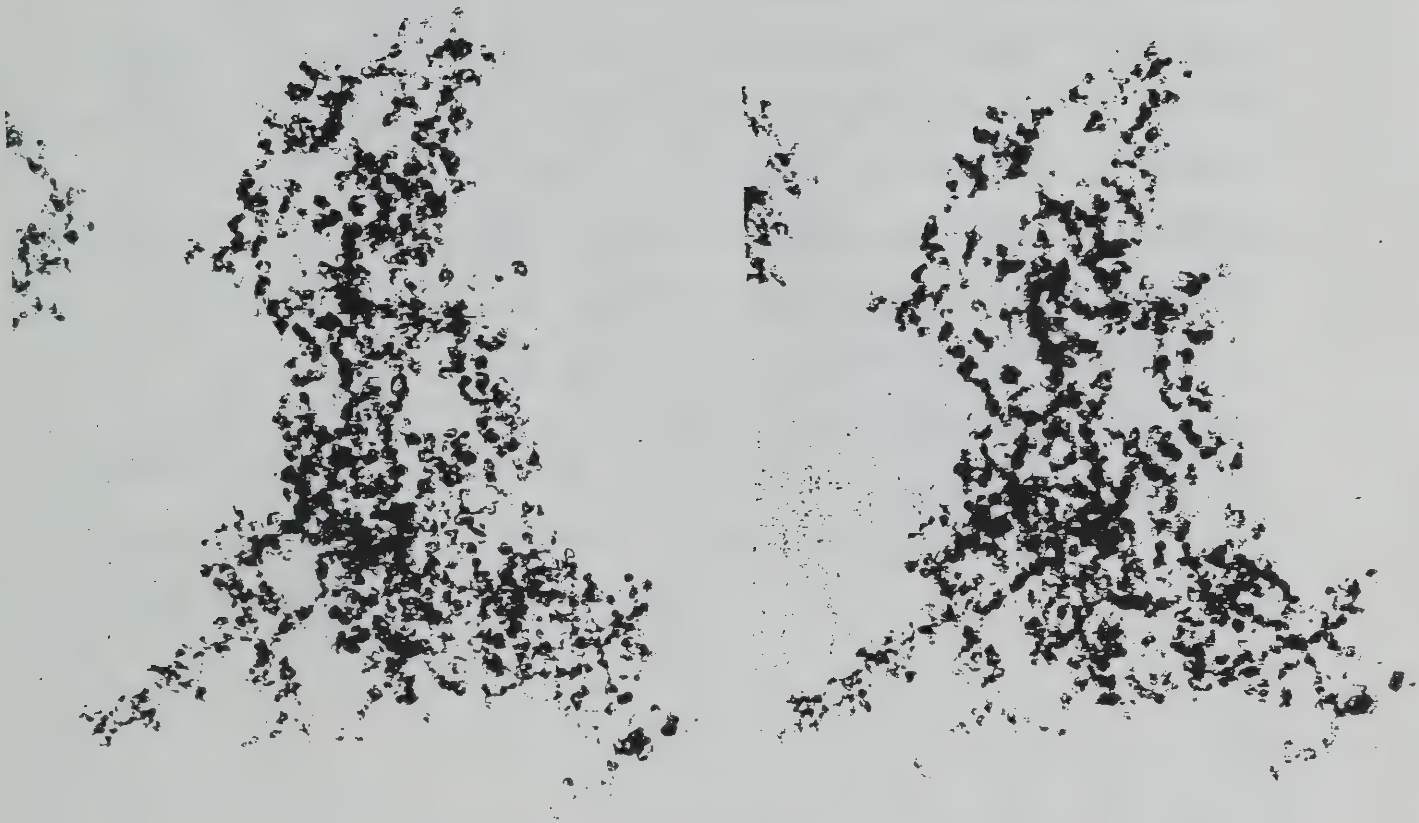

Figure 10. Stereopair of the agglomerate shown in figure 9.

is assigned a value of 155, all pixels with levels from 155 to 255 are reset to 255 (white), while pixel gray levels from 0 and 154 are set to 0 (black). We note that the micrographs are negatives whereby clusters are light gray set against a dark background. The end result is a 512 x 512 array representing the threshold version of the digitized image. For simplicity, values of 255 are set to 1.0 so the array consists of only 1's and 0's. Array values of 1.0 are termed 'occupied sites' since thay signify the presence of a particle, in either a portion or its entirety, at that location. Surrounding clusters not associated with the cluster of interest are eliminated from the threshold version by assigning corresponding pixels a value of 0.0 through Lispix. Data in this category are evaluated by the successive square, pair correlation, and Sullivan [1985] methods.

V. Data Analysis

In this section, the techniques used to determine D_f will be discussed in greater detail. We noted in the previous section that all the data pertaining to the D_f were obtained from TEM micrographs of agglomerates. Consequently, it is our goal to obtain 3-D structural information from the 2-D TEM images. The data analysis procedures to be discussed later in this section depends on the assumption that essentially all particles are evident in the projection, i.e. that the agglomerate is transparent and only a few particles are completely masked by others. The validity of this assumption relies on the fractal dimensionality being less than 2.0, which is believed to be the case for agglomerates. Mandelbrot[1977] states that $D_f < 2.0$ implies that the projection typically itself is of dimension D_f. Weitz and Huang[1984] offers a simple argument based on the relation

$$M \sim R^{D_f} \qquad (19)$$

which is the same form as equation 1 but N is replaced by the cluster mass M. Upon projection, M does not change, while in two dimensions normal to the projection, R also remains constant. Thus the projection remains a fractal, with the same D_f, provided the mass can be measured. This will be possible only if there is not too much overlap in the mass, which produces the condition $D_f \leq 2$. We shall further discuss the validity of this statement in light of the analysis of simulation clusters in 3-D and their projections, in addition to the previous verification of TEM results by small angle neutron scattering measurements in a study of gold colloid agglomeration.

A. Particle Counting Method

In this method, the total number of primary particles are determined as a function of cluster size. The clusters chosen are limited to those consisting of 200 particles or less, beyond which one encounters increasing difficulty in distinguishing overlapping and partially fused spheres, even with stereoscopic pairs. Two definitions of cluster size are used (see figure 9): the first is in terms of the geometric mean of the cluster length L, and W, the projected length perpendicular to the axis through L, and the second definition in terms of the radius of gyration R_g, as given by

$$m_T R_g^{2} = \sum_{i=1}^{N} (m_i r_i^{2}) \tag{20}$$

where m_T is the total mass of the cluster and m_i is the mass of particle i whose center is at a distance r_i from the centroid. It was assumed that all m_i's were equal, making m_T directly proportional to the total number of particles N. However, particle diameters actually varied by as much as 16% within a cluster. In an attempt to minimize the error introduced by this assumption and also to account for different magnifications, R_g, as measured from the photograph, was normalized by dividing its value by the average particle diameter $\bar{d}$. Values of $\bar{d}$ were obtained by arbitrarily choosing 10 representative primary particles from each cluster. The geometric mean $(LW)^{1/2}$ was normalized in the same fashion as R_g. A useful quantity is the ratio L/W, which provides a description of overall cluster shape. To test whether the cluster growth is fractal, we plotted log(size) versus log(N). For fractals a linear dependence with a slope of D_f^{-1} will be observed (see equation 1).

B. Analysis of Large Clusters (5-40 μm)

1. Successive Squares Method

As previously mentioned the digitized data from electron micrographs of large clusters consisted of 512 x 512 arrays with values of 1's (occupied site) or 0's (unoccupied site). The first method to evaluate D_f from this data set involved placing series of non-overlapping squares of side ℓ from the center of mass of the agglomerate. The total number of sites occupied within each square is then determined as a function of ℓ. This is similar to the Nested Square method of Forrest and Witten [1979], except that the center of all the squares are the same in our analysis. In the Nested Squares method, the square center location was chosen as the point where the center of mass of occupied sites within the square and the geometric center of the square coincided. We found no theoretical justification for doing the same. For a fractal, N will vary as ℓ^{D_f}. A weighted fit of log(N) versus log(ℓ) was perfomed, assuming that the square of the probable error for each point varied as $N^{-1/2}$. A listing of the successive squares computer code is given in Appendix A.

2. The Pair Correlation Method

In this method, the pair correlation approach was used to find D_f. By definition, c(r) is the average density of occupied points in the digital image at a distance of r from each occupied point. The use of a 512 x 512 lattice, however, places a limit on the number of points (occupied or unoccupied) that are a distance of r around each point. Consequently, we approximate this density as the density of occupied sites in a shell of inner radius r-0.5 and outer radius r+0.5. From equation 5, c(r) is determined by averaging the density at r over all occupied sites. This is done for a reasonable range of r values (1-200 pixel spacings). For a fractal, c(r) should vary as $r^{D_f - d}$, where d=2. Since the clusters are of finite size, it is also expected that equation 5 will be valid for a short range of r, since for longer r values, larger areas outside the edge of the agglomerate are encountered.

A computer program is used to compute c(r) (Appendix B). In the program, the distances between each and every particle, rounded-off to the nearest integer, is determined. Then the number of occurences of each distance is recorded in array n(i). If n(51)=2100, for example, the total number of times when an occupied site is at a distance of r ~ 51 to another occupied site is 2100. The value of c(r) is computed by dividing n(i) by the total number of occupied sites N and by the total number of points (occupied or unoccupied) in a shell of inner radius r-0.5 and outer radius r+.5 in a square lattice.

3. The Sullivan Approach

The third and final method used for the 512 x 512 data set is a program developed by Sullivan[1985]. It makes use of a tree method which efficiently stores important structural information. This procedure can be best described by considering a 1 dimensional fractal set (i.e. N points scattered along a straight path) between points x_1 and x_2:

.. ..

x_1 x_2

The set is normalized by scaling the minimum (x_1) to zero and the maximum (x_2) to 1.0. Therefore, all the points belonging to the set are represented by a fraction between 0 and 1:

.. ..

0 0.5 1

The point locations are then converted to binary fractions (i.e. 1's and 0's). For example, if $x=.25$, the corresponding binary fraction is '01' since $.25= 0*(1/2)^1 + 1*(1/2)^2$, and $x=.75$ has a binary fraction of '11' since $.75 = 1*(1/2)^1 + 1*(1/2)^2$. These binary fractions represent directions or paths each point follows when a hypothetical tree is constructed.

Consider the tree depicted in the following figure:

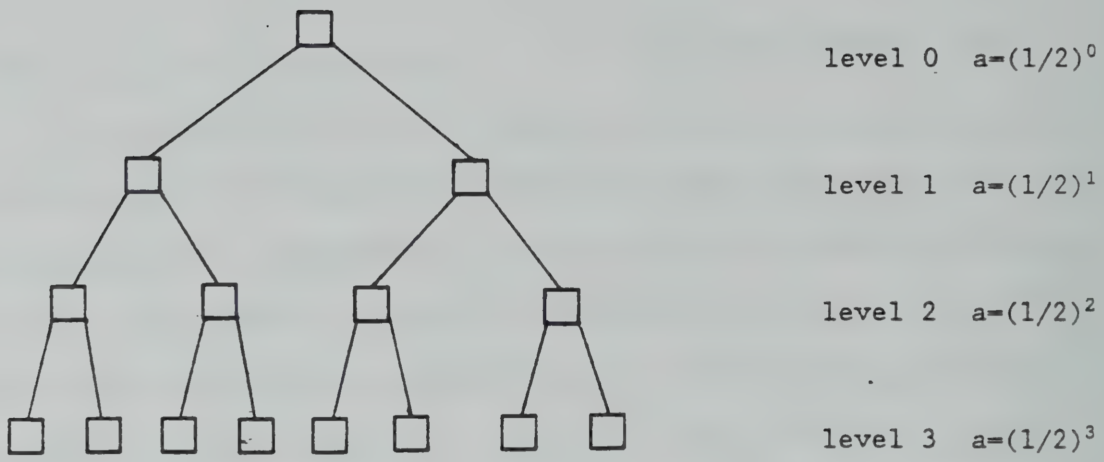

Starting at level 0, each point has a unique path to follow which is defined by its binary fraction. The binary sequence is read from left to right, designating a value of 1 as a direction downward to the right, and 0 as a direction downward to the left. Taking x = '01', for example, the path

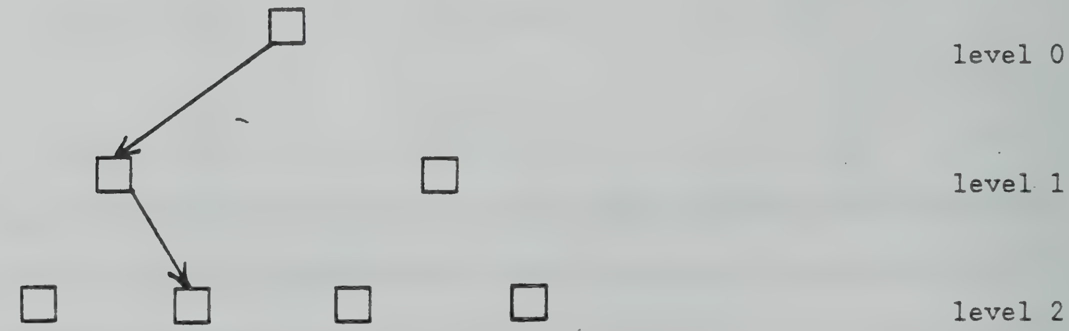

is followed (shown by the dark arrows). The procedure is repeated for each point, while storing the number of 'hits' to the boxes in each level. At level 2, there are 4 boxes:

The number of hits contain information on how the set is structured. The hits in box a, for example, represent the number of points between 0 and 0.25, in box b, between .25 and 0.5, in box c, between 0.5 and 0.75, and in box d, between 0.75 and 1.0.

Recall equation 3,

$$K(\underline{a}) = \underline{a}^{-D_f} \tag{3}$$

where $K(\underline{a})$ is the number of segments (in 1 dimension) of length $\underline{a}$ needed to cover the set. The tree, as constructed, actually represents each level as $\underline{a} = (1/2)^{\text{level \#}}$. The number of boxes that have been hit at each level is $K(\underline{a})$. Thus the fractal dimension can be computed from the slope of $\log(K(\underline{a}))$ versus $\log(\underline{a})$. The program computes D_f from $K(\underline{a})$ and $\underline{a}$ at each level. The error in D_f decreases as the number of boxes in each level approaches the total number of occupied sites N.

The tree concept provides an efficient algorithm that has a short execution time since $K(\underline{a})$ is computed at values of uniform distribution in a log-log plot, and is suitable for vector programming on the Control Data Corporation Cyber 205 supercomputer. The actual program used is a similar version but is applied to two dimensional fractals. The x and y coordinates are scaled from 0 and 1, but the tree is instead constructed of 4 possible branches per box, i.e. for the x and y binary:

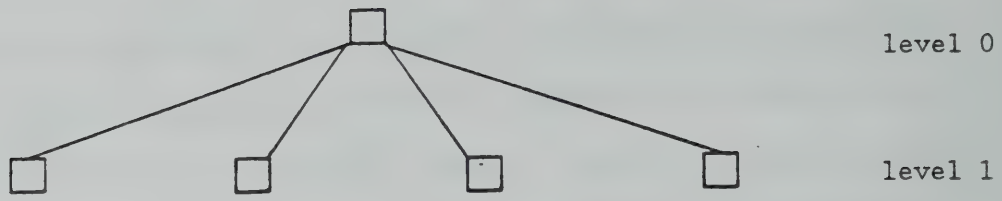

The pair correlation and Sullivan's method were verified using a two dimensional fractal known as a Sierpinski carpet with a fractal dimension $D_f \sim 1.89$ (see section II), along with compact ordinary objects with $D_f=d=2$. The fractal dimensions computed were within 2% of the true values. In the next section, the experimental values of D_f for the soot agglomerates, along with other structural features are presented. These results are then compared with simulations and past experimental studies of inorganic smokes and gold colloids.

VI. Results

A. Particle Counting Method

Thirty seven clusters were collected and evaluated by the particle counting method. Table 2 is a listing of cluster size as a function of N for a few of the samples collected. Our own ability to distinguish individual particles limited the size range to $5 \leq N < 200$, even with stereopairs. The results are summarized in figure 11. The linearity observed indicates a mass-size power law relationship described by equation 1. Fractal dimensions of 1.61 ± .13 and 1.49 ± .16 for cluster sizes defined by $(LW)^{1/2}$ and R_g, respectively, were obtained by linear regression. A rather diverse set of shapes (L/W), from those of high sphericity ($L/W \sim 1.0$) to those approaching linearity ($L/W > 2$) were observed. The average agglomerate length to width ratio was 1.68 ($\sigma = 0.50$).

In view of our expectation that the number of particles counted may be low for large agglomerates due to the obscurity of particles, it is reasonable to expect the slope of both experimental lines to be slightly lower than theoretically expected for a fractal. As seen in figure 9, there are certain regions of high overlap where undercounting is likely. Below we show how undercounting of N will further reduce the value of D_f when using R_g as cluster size.

We let n represent the difference between the actual number of spheres, N, and the measured number, N_m. Expressing equation (20) in terms of N, N_m, and n, we obtain

N	$\bar{d}$ (nm)	^{a} (nm)	$R_g/\bar{d}$	$(LW)^{1/2}/\bar{d}$	L/W^{b}
5	27.9	2.0	.55	2.33	1.15
10	30.9	4.1	1.56	3.93	1.91
13	28.7	2.9	1.19	4.46	1.29
14	28.5	3.5	1.18	4.24	1.33
21	25.5	2.0	1.85	5.96	1.39
22	21.1	2.0	1.41	4.97	1.24
23	34.2	2.3	2.12	5.57	1.72
31	26.2	3.5	2.05	6.53	1.02
39	22.0	1.7	2.27	6.33	1.88
46	27.3	2.7	3.11	8.68	1.58
52	23.8	2.9	2.87	9.30	1.08
56	29.3	2.0	2.98	9.57	1.08
57	26.4	2.4	3.21	9.06	1.88
68	30.6	3.0	4.22	12.7	1.33
82	22.1	3.0	4.82	12.4	1.74
99	35.8	2.7	4.62	13.1	1.68
107	41.6	8.8	5.25	14.0	1.50
109	31.4	3.9	6.24	14.3	2.79
162	34.8	9.3	7.45	22.4	1.21
164	28.1	3.9	7.12	19.2	2.06

Table 2. Typical results for the particle counting method.

[a] σ refers to the standard deviation of mean d.

[b] average L/W for entire set is 1.68, $\sigma = .50$

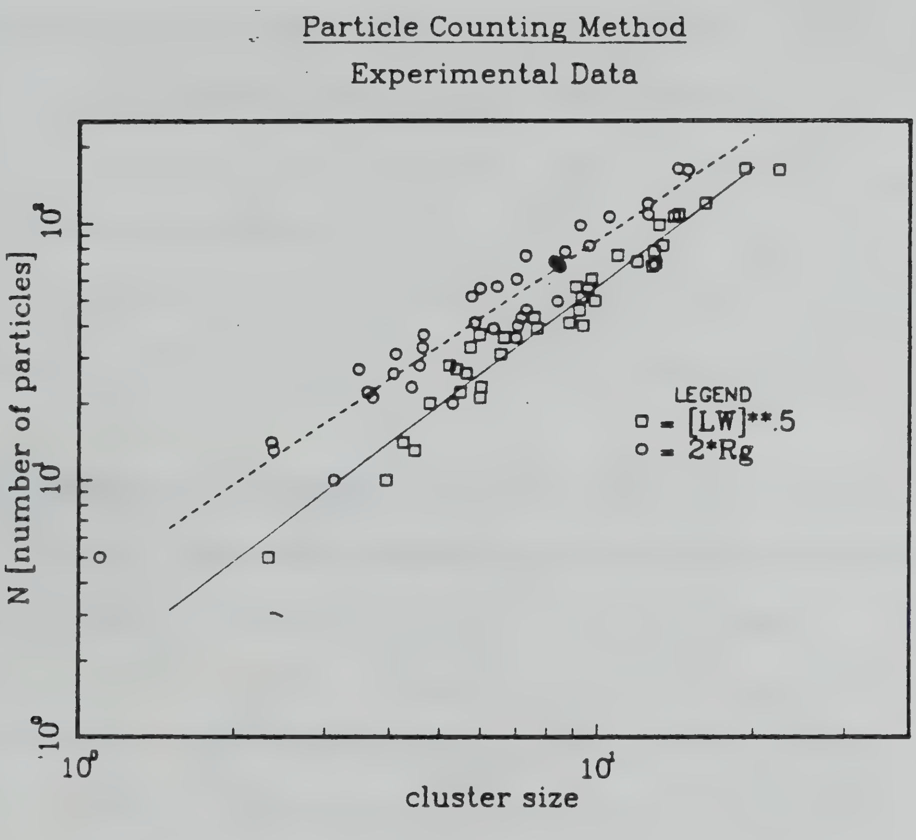
Particle Counting Method

Experimental Data

Figure 11. R(size) vs N for experimental data. Cluster sizes defined as R_g or $(LW)^{1/2}$.

$$NR_g^{\,2} = N_m R_{gm}^{\,2} + \sum_{i=1}^{n} r_i^{\,2} \tag{21}$$

where R_{gm} is the measured radius of gyration and r_i now represents the distance from the center of mass to the i^{th} sphere ($i=1$ to n) not accounted for in the measurement. Rearranging equation (21),

$$R_g/R_{gm} = N_m + \left[\frac{(\sum_{i=1}^{n} r_i^{\,2})/R_{gm}^{\,2}}{N_m + n}\right]^{1/2} \tag{22}$$

A two-term Taylor series expansion is performed to obtain a simplified expression adequate for making qualitative comparisons:

$$R_g/R_{gm} \approx 1 + 1/2\left[\frac{(\sum_{i=1}^{n} r_i^{\,2})/R_{gm}^{\,2} - n}{N_m + n}\right] \tag{23}$$

In general, we observed that overlaps are present near the agglomerate center of mass. Now consider a situation where 20% undercounting has occured, i.e. $N_m = 0.8N$ and $n = 0.2N$. For the extreme case of $r_i=0$ (overlaps at the center of mass), we get, from equation 21,

$$R_{gm} \approx 1.11R_g \tag{24}$$

and for $r_i \sim 0.5R_g$,

$$R_{gm} \sim 1.08R_g \tag{25}$$

Equations 22 and 23 show that undercounting further aggravates the slope D_f by yielding superficially higher R_{gm} values. It is therefore expected, as supported by figure 12, that a lower slope of D_f will result using R_g as cluster size as opposed to $(LW)^{1/2}$. The errors introduced will be more pronounced for elongated structures, typical of those which where evaluated. On the other hand, note that the measured $(LW)^{1/2}$ is independent of the fraction of particles undercounted.

B. Pair Correlation, Sullivan, and Successive Squares Method

In table 3 , the results of the pair correlation, Sullivan, and successive squares methods are listed for the size range 5.5 to 38 μm. Agglomerates quite similar in shape to those of the particle counting method were collected (i.e. elongated and spherical) but on a much larger scale. The average length to width ratio of these agglomerates was 1.8 (σ=0.66). Table 3 shows that from each of the three methods, the agglomerates have fractal dimensions between 1.75 and 1.95.

The pair correlation function showed the greatest sensitivity towards the internal structure and overall shape of the agglomerates. The power law dependence of c(r) on r clearly suggests fractal behaviour in terms of the scale invariant internal structure of the agglomerate.

However, that range of r where equation (7) is valid appears to be strongly dependent on the shape (L/W). Figures 12a and 12b are examples of clusters with high sphericity (L/W = 1.1 and 1.2) where power law is observed over a long range of r (2-37 and 2-24). On the other hand, cluster number 2513 (L/W = 2.9) shown in figure 12c is at best linear for the range r=2-7. This is probably due to the fact that for elongated structures a greater percentage of the area around the edges are encountered as opposed to rounded ones. These areas of zero density significantly lower c(r) as seen in all cases as r approaches the size of the agglomerate. By the same token, smaller agglomerates (< 5 μm,) such as cluster number 2500 shown in figure 12d whose internal structures are not yet fully developed also display shorter power law ranges. Weitz and Huang[1985] compensated for this effect by considering occupied sites only a short distance from the center of mass. A summary of the effects of cluster size and shape is illustrated in figure 13a, a combined plot of c(r) versus r for r=1 to 250. Those agglomerates with L/W~1 are shown to have longer power law dependence which is followed by a steeper drop for large r when edge effects are encountered. Elongated or underdeveloped structures followed a gradual decline towards the limiting value of c(r)=0. As a test case, c(r) was determined for a solid square (L/W=1.0) and rectangle (L/W=3.0) of similar sizes. The result is plotted in figure 13b. For slopes equal to 1.98 ± .01, a longer range of linearity is found for the square. The long range effects of shape on c(r) may not have any direct bearing on D_f. This information, however, may prove to be useful in any future work regarding light scattering of particles of such shapes and sizes.

image number	magnification (KX)	c(r)	Df	
			sullivan	nested
2313-115[b]	10	1.82 ± .02	1.82	1.86
-120		1.81 ± .02	1.81	1.88
-125		1.80 ± .02	1.80	1.83
2315	10	1.81 ± .02	1.81	1.87
2500	7.3	1.80 ± .05	1.77	-
2509	6	1.86 ± .02	1.84	1.94
2510	5	1.81 ± .01	1.83	-
2507	5	1.93 ± .01	1.87	1.95
2504	2	1.85 ± .02	1.83	1.79
2505	2	1.91 ± .01	1.85	1.95
2506	2	1.92 ± .01	1.87	1.92
2516-0°	2	1.94 ± .01	1.88	1.95
-45°		1.94 ± .01	1.90	1.95
2512	1.5	1.90 ± .01	1.83	1.83
2515	1.5	1.90 ± .01	1.81	1.66
2513	1.5	1.84 ± .06	1.76	1.82
test images				
Sierpinski Carpet		1.86 ± .02	1.90	-
square		1.98 ± .01	2.00	2.00
rectangle		1.98 ± .01	2.00	2.00

Table 3. Calculated values of the fractal dimension D_f

[a] mean L/W = 1.8 $\sigma = .66$

[b] 115,120, and 125 are threshold gray levels.

table 3. continued

image number	number of occupied sites	range of r in c(r)	$(LW)^{-1/2}$ μm	L/W[a]
2313-115[b]	39708	2-23	7	1.1
-120	37721	2-26		
-125	35804	2-24		
2315	30067	2-25	5.5	1.6
2500	25453	2-11	7.3	1.5
2509	33620	2-20	9.1	3.0
2510	39489	2-37	12.0	1.1
2507	72890	2-23	13.8	1.3
2504	29916	2-22	22.0	1.8
2505	49266	2-30	24.6	1.9
2506	63472	2-24	36.1	1.2
2516-0°	72358	2-21	35.5	1.1
-45°	69776	2-22	30.0	1.4
2512	27858	2-17	33.2	2.5
2515	29303	2-16	29.2	2.1
2513	19701	2-7	38.0	2.9
test images				
Sierpinski Carpet	32768	2-10		1.0
square	155236	1-18		1.0
rectangle	154184	1-15		3.0

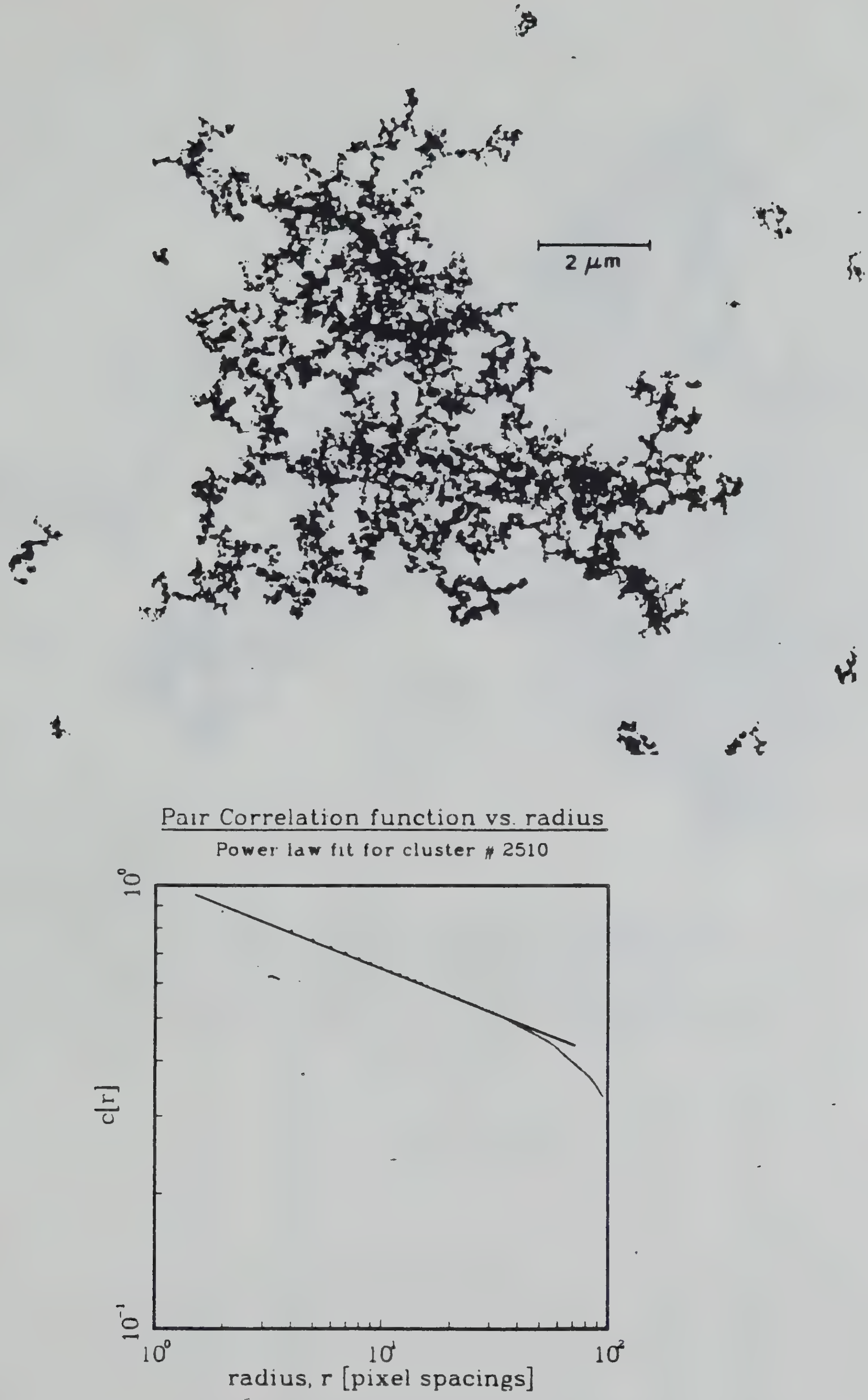

12(a). L/W=1.1, $(L/W)^{1/2}$=12.0 μm, fit r in range 2-37.

Figure 12(a-d). Micrograph and associated c(r) plot for a variety of agglomerate shapes.

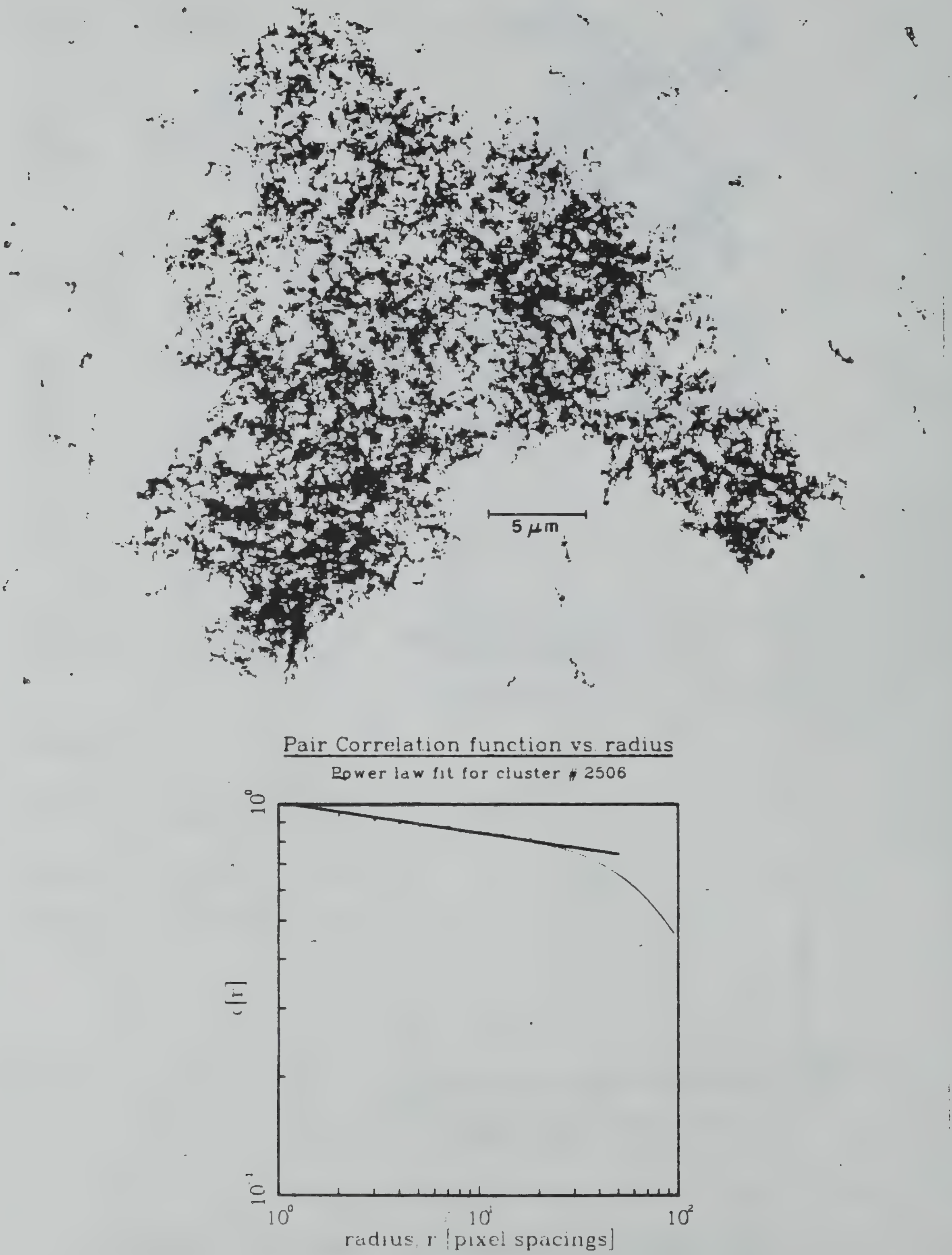

12(b). L/W=1.2, $(L/W)^{1/2}$=36.1 μm, fit r in range 2-24.

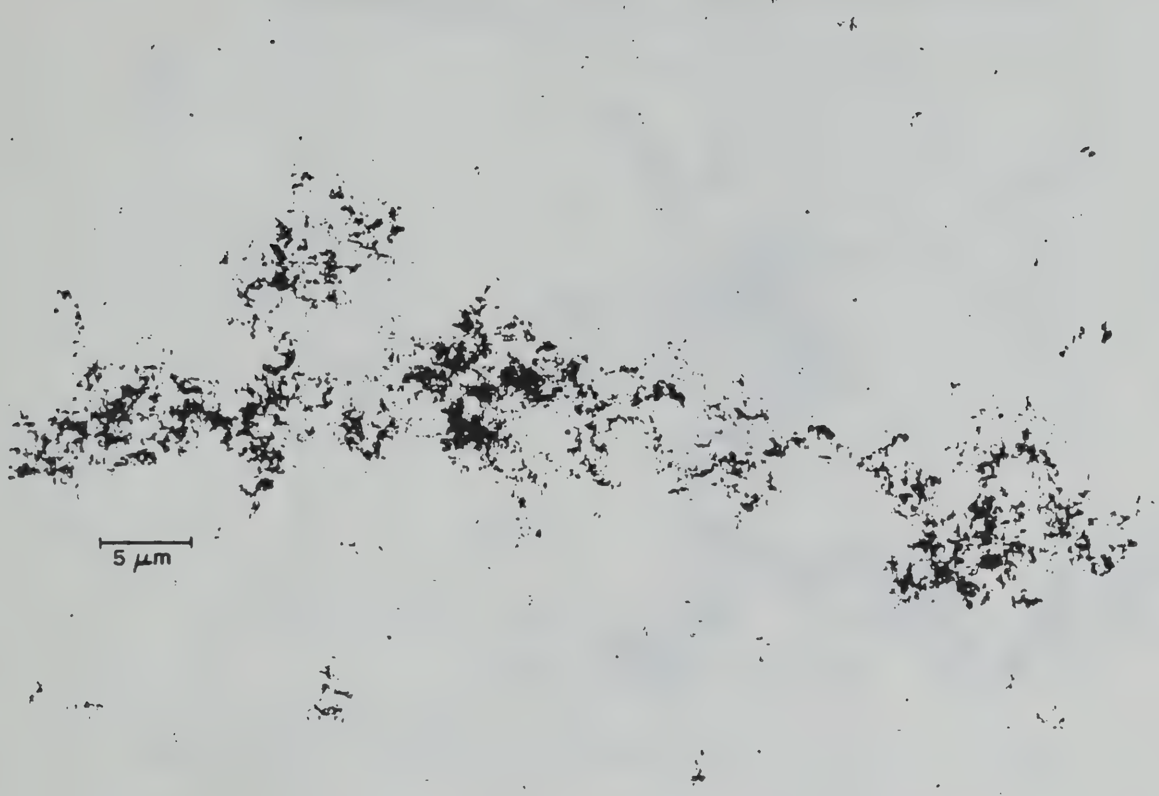

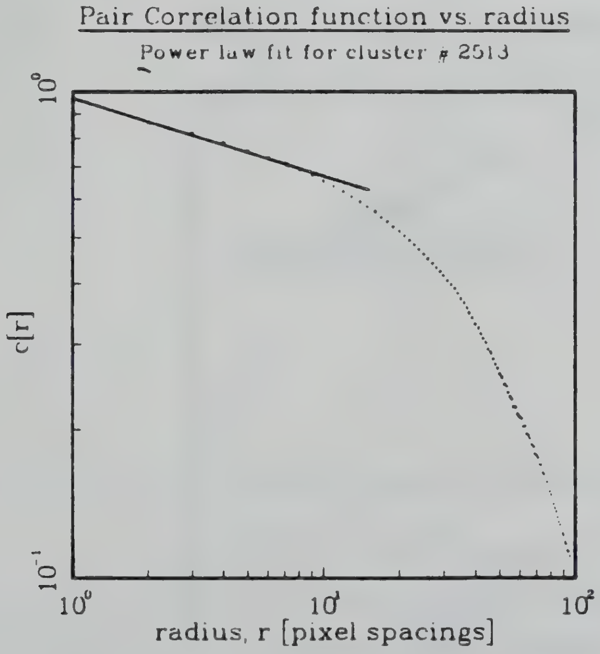

12(c). L/W=2.9, $(L/W)^{1/2}$=38.0 µm, fit r in range 2-14.

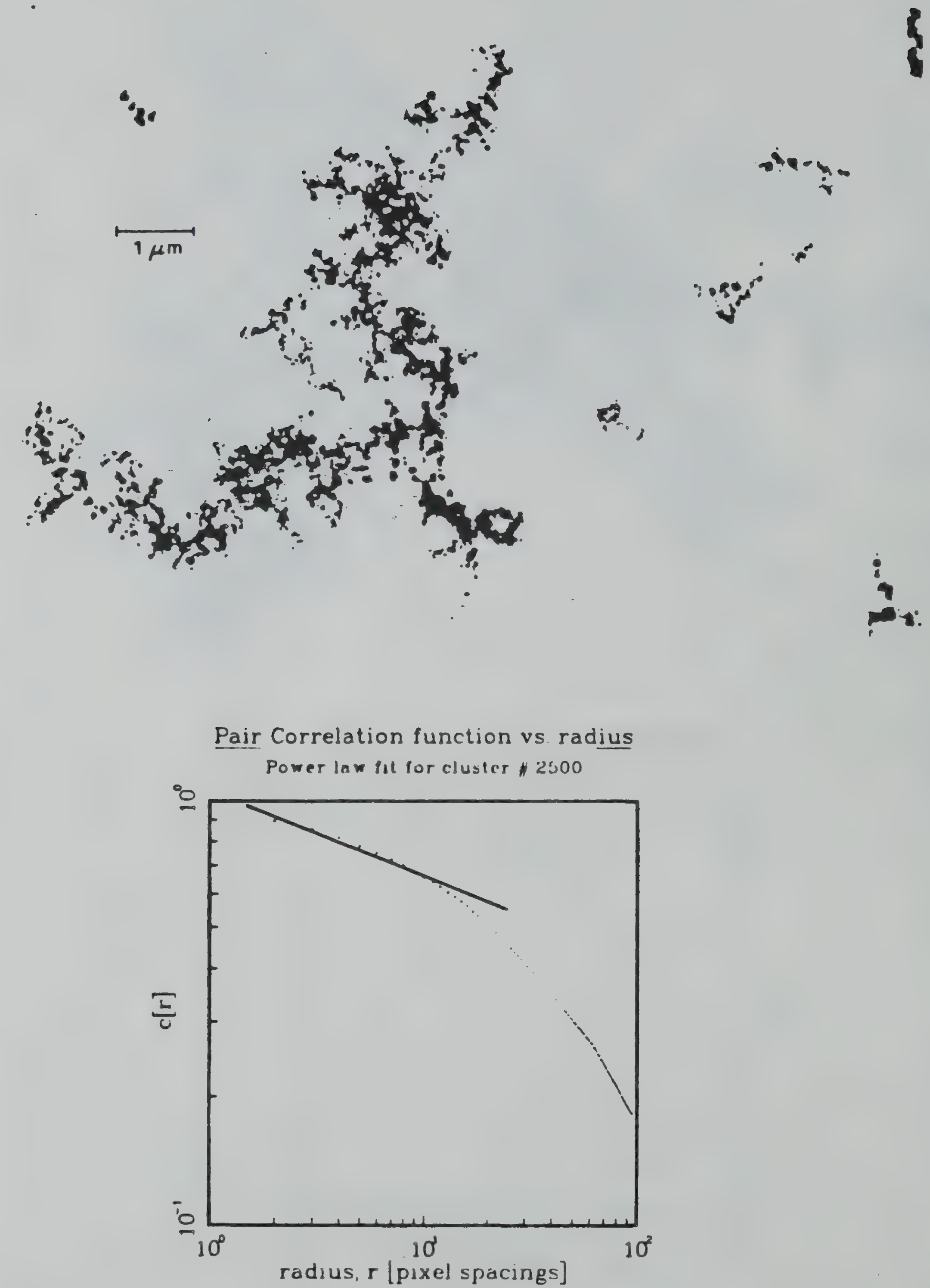

12(d). L/W=1.5, $(L/W)^{1/2}$= 7.3 μm, fit r in range 2-7.

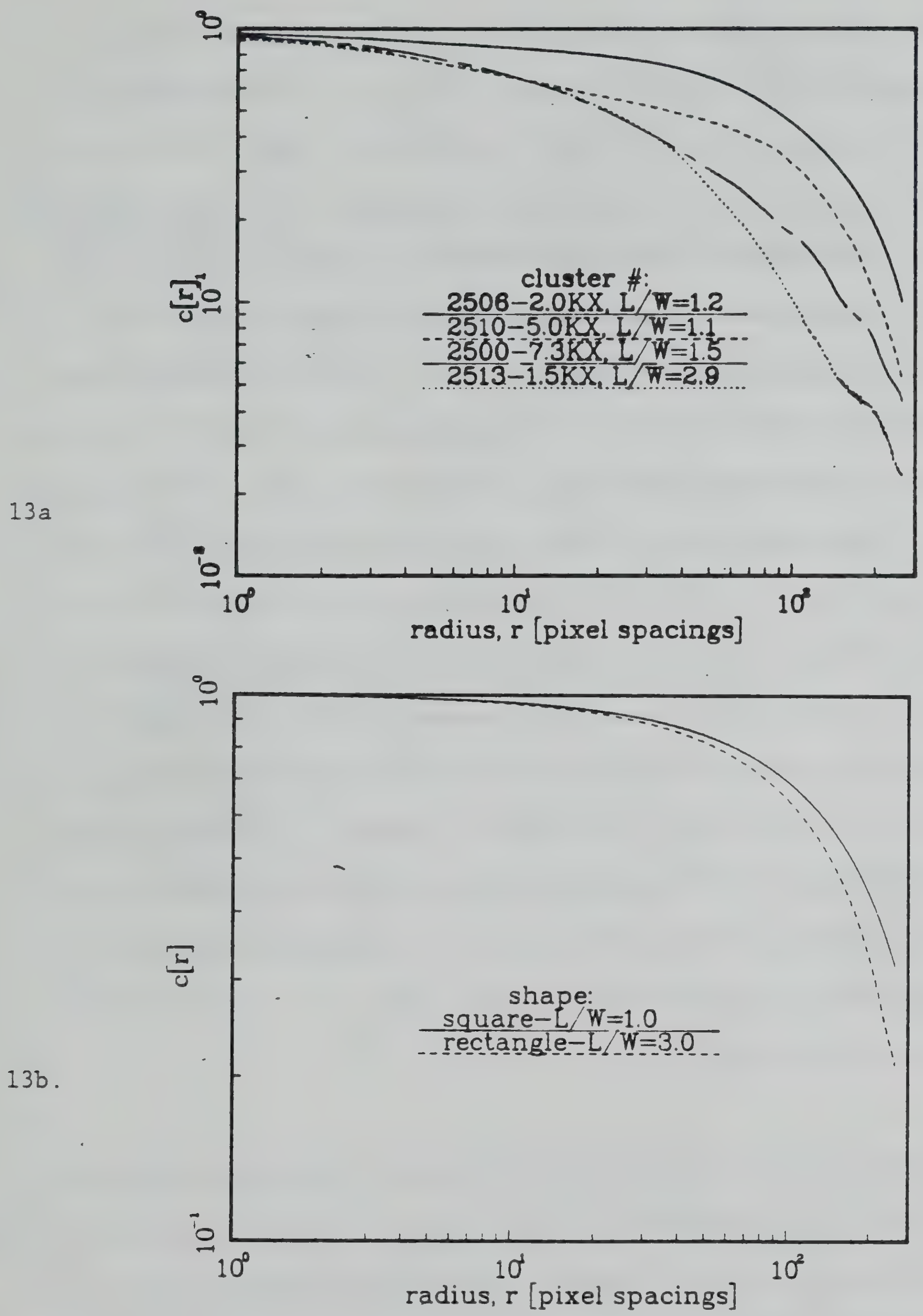

Figure 13. Long range effects of shape on c(r). (a) combined c(r) plots for clusters in previous figures, and (b) test case for filled Square (L/W=1) fit r in range 1-18, Df=1.98 ± 0.01, and filled rectangle (L/W=3.0), D_f=1.98 ± 0.01, fit r in range 1-15.

There is very good agreement between the pair correlation and Sullivan approach for clusters between 5 and 12 μm, corresponding to magnifications between 5 and 10 KX, respectively. Below 5 KX, however, D_f by the c(r) approach becomes consistently higher (by ~.05) than those of greater magnification. It appears that the digitized images become denser for agglomerates larger than about 12 μm, most of which are photograped at magnifications less than 5 KX. First we consider the possibility that the increased D_f for agglomerates of sizes > ~12 μm be the result of instrument limitations or events unrelated to the growth phenomena. More specifically, there is an inherent decrease in resolution on a 512 x 512 lattice as more than one particle begin to occupy each pixel. Table 4 shows the approximate length between pixels in comparison with the average particle diameter at different magnifications. At about a magnification of 5 KX, the length of one side of an occupied site is about equal to a particle diameter. The resolution further diminishes at 2 KX where void spaces between the particles must have areas greater than that projected by ~2.4 neighboring particles to be distinguished as occupied sites. For 1.5 KX , this area increases to 3.2 neighboring particles.

To more accurately measure the effects of decreasing resolution, the 512 x 512 array representing cluster number 2313 was reduced to a 256 x 256 array of 1's and 0's. This was done by checking groups of 2 x 2 pixels in the 512 x 512 array for ≥ 50% occupancy (values of 1's). If ≥ 50% occupied, the corresponding location in the 256 x 256 matrix is set to 1.0, otherwise it is 0. In effect, a 256 x 256 matrix is obtained

TEM Magnification	number of pixel lengths equalling one particle diameter (30nm)
10 KX	2.1
7.3 KX	1.6
6 KX	1.3
5 KX	1.0
2 KX	0.4
1.5 KX	0.3

Table 4. Resolution of mass in digitization process.

just as if the micrograph was digitized with such a resolution. The procedure is repeated to obtain a 128 x 128 and 64 x 64 matrix. The data was then evaluated the c(r) method. As shown in figure 14, the power law slope is essentially the same for all four curves. Although deviations from power law behaviour appear at different r values, these would actually correspond to approximately the same lengths if plotted versus micrometers. We therefore conclude that the effect of low resolution does not result in a superficially higher D_f as suggested. In retrospect, if the agglomerates are indeed fractals, the internal structure is statistically scale invariant and changes in length scales (varying resolution) would unaffect D_f. Whether bigger clusters result in larger exponents, which implies that some other physical mechanism takes over, will be discussed in the next section in light of computer simulations of cluster-cluster agglomeration.

To examine the possible effects of the imaging process on D_f, variations in threshold levels and tilt angles were investigated. Micrograph number 2313 was processed at threshold levels 120, 125, and 130, and only a 1% change in D_f was found by the pair correlation and Sullivan methods. In general, a threshold value within ± 5 gray levels of those that represent a contiguous image adequately resembling a silhoutte of the agglomerate is chosen. In terms of the tilt angle, no significant effect was also found. Cluster number 2313 was tilted 55° and is represented by cluster 2315. As an aside, one can infer that the agglomerate extends out in all three directions as opposed to two. If growth proceeded along a plane, one would expect a prominent increase or

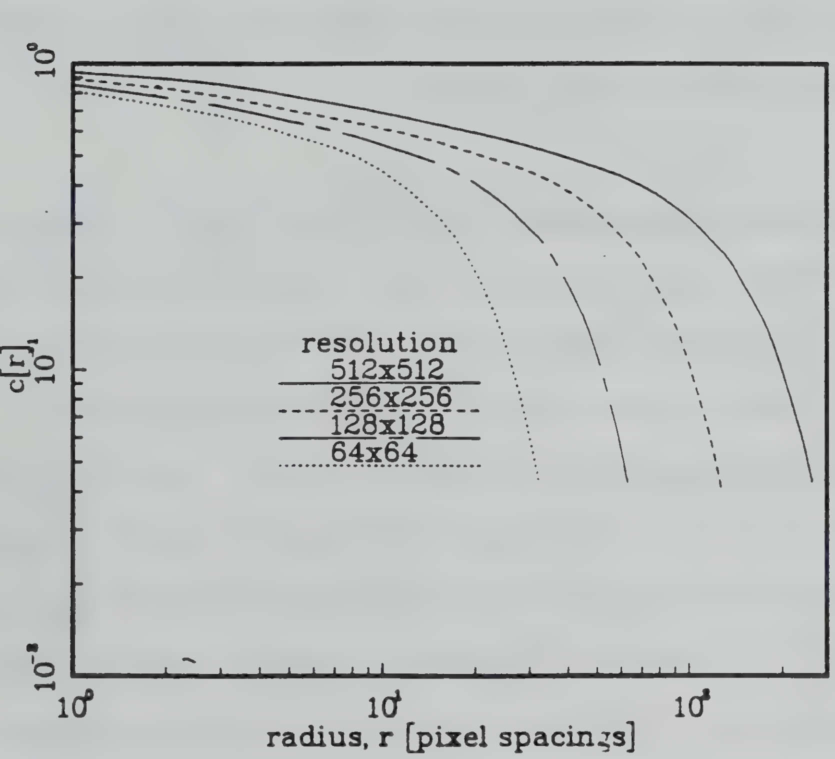

Figure 14. Effect of digitizer resolution on c(r) fit for all lines yield slopes $D_f \sim 1.80 \pm .02$.

decrease in size as the sample is rotated, which is certainly not the case for clusters 2313 and 2516 upon rotation. This also upholds the assumption that the sample is not distorted or flattened on the TEM grid, which was the case for gold colloids when dried during sample preparation. These results indicate a moderate insensitivity towards thresholds and tilt angles. Consequently, the analyst has greater flexibility and control in the digitization process.

Generally higher values of D_f resulted from the successive squares method. Figure 15 is a plot of log(N) versus log(ℓ) with a slope of D_f=1.83. This method, however, was found to be ineffective for clusters where the center of mass is in a region of unoccupied sites, characteristic of small agglomerates with few branches, resulting in non-linearity. In regard to computer execution times, Sullivan's approach was found to be at least two orders of magnitude faster than the c(r) method. The advantage of the c(r) method, however, becomes apparent when insight into the contribution of individual particles to total scattering is desired.

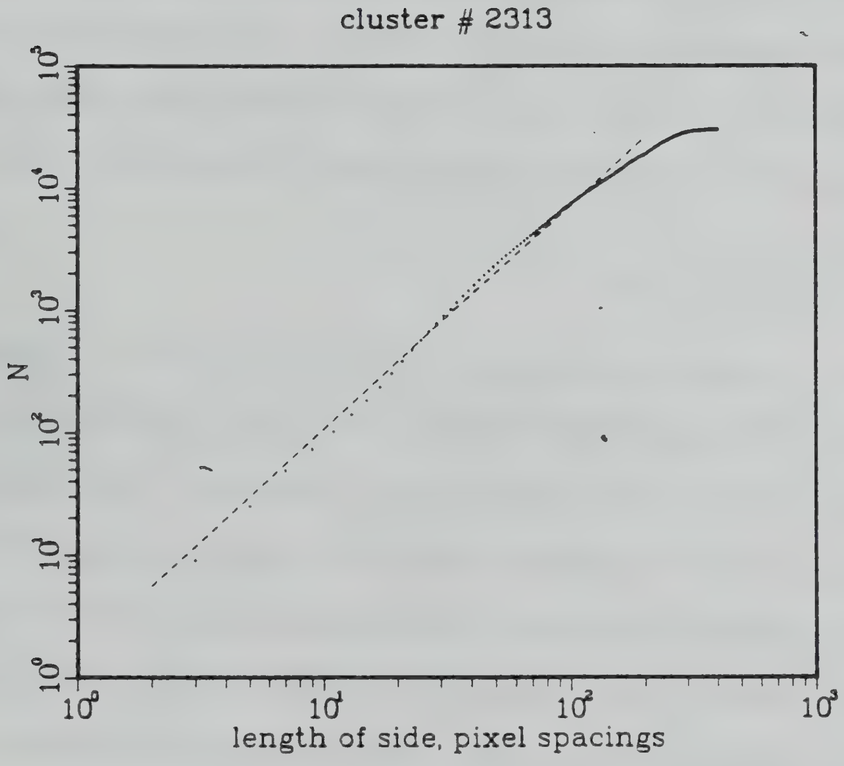

Figure 15. Successive Squares method plot, Fit for ℓ=2-181, slope D_f=1.82.

VII. Discussion

The results given in the previous section now permits a qualitative and quantitative look at actual and predicted properties of agglomerate growth and morphology. Figure 16 shows comparative sizes of clusters obtained experimentally and those generated by DLA and cluster-cluster agglomeration. Note the similarities between the open and chain-like structures of experimental and cluster-cluster agglomerates. DLA aggregates appear more dense and compact, characteristic of its high dimensionality of 2.50. On the basis of appearance alone, it is obvious that cluster-cluster agglomeration best represents the soot agglomeration process.

For a quantitative comparison, we applied the D_f methods of analysis to the simulation clusters. We first address the question of whether D_f is indeed invariant upon projection by applying the particle counting and pair correlation method to clusters generated from Mountain and Mulholland's simulation. The availability of their program provided the opportunity to vary operating parameters such as the aerosol relaxation time and particle density. Table 5 shows the results of the analysis for $\beta\tau$=.05 and ρ=.0167. For the particle counting method, the results indicate a 3-4% decrease in D_f when evaluating projections instead of actual 3-D coordinates. Accounting for the errors in the slope of the N vs. R_g plot, however, makes this difference relatively insignificant. To test the pair correlation approach, a 'digitized' projected image was created from a Monte-Carlo integration technique

	D_f	
particle counting	3-D	projected 3-D
$2 \leq N \leq 200$	1.71 ± .06	1.63 ± .08
$2 \leq N \leq 2000$	2.00 ± .04	1.94 ± .05
pair correlation		
N=1590	1.65 ± .20	1.67 ± .04 (digitized projection)

Table 5. Comparison of 3-D and projected values of D_f from cluster-cluster simulation.

listed in Appendix D. As seen in table 5, there is good agreement between D_f in two and three dimensions.

Experimentally, we obtained a D_f of 1.49 ± .13 and 1.61 ± .08 by the particle counting method for the set of agglomerates in the range $5 \leq N < 200$ for cluster sizes defined as R_g and $(LW)^{1/2}$, respectively. Large experimental clusters from 5 to 15 μm were stated to have a dimensionality $D_f \sim 1.85$ by the pair correlation and Sullivan methods. No corresponding increase in D_f was experienced for the diffusion limited aggregation model. In DLA, for example, the pair correlation analysis of a cluster of ~3000 particles yielded similar D_f values (~2.4) as that obtained for an R_g vs k plot for $1 < k < 200$ particles. In contrast, cluster-cluster agglomerates exhibited a dimensionality of 1.70 for $2 \leq N \leq 200$ and 2.00 for $2 \leq N \leq 2000$ by the particle counting method as previously mentioned. This apparently suggests an increase in D_f as observed experimentally. However, there is greater scatter in the data for large N since fewer of these clusters are formed. This result is still therefore inconclusive. Figure 17 is a comparison of experimental and simulation data for the particle counting method. The much steeper slope for DLA is obviously the result of its denser structure. The fitted equations for both simulations are also valid for k up to about 200 particles.

It was also reported that clusters > 12 μm had slightly larger D_f values (~1.9). A decrease in digitization resolution was dismissed as an explanation for this finding. It is therefore probable that either

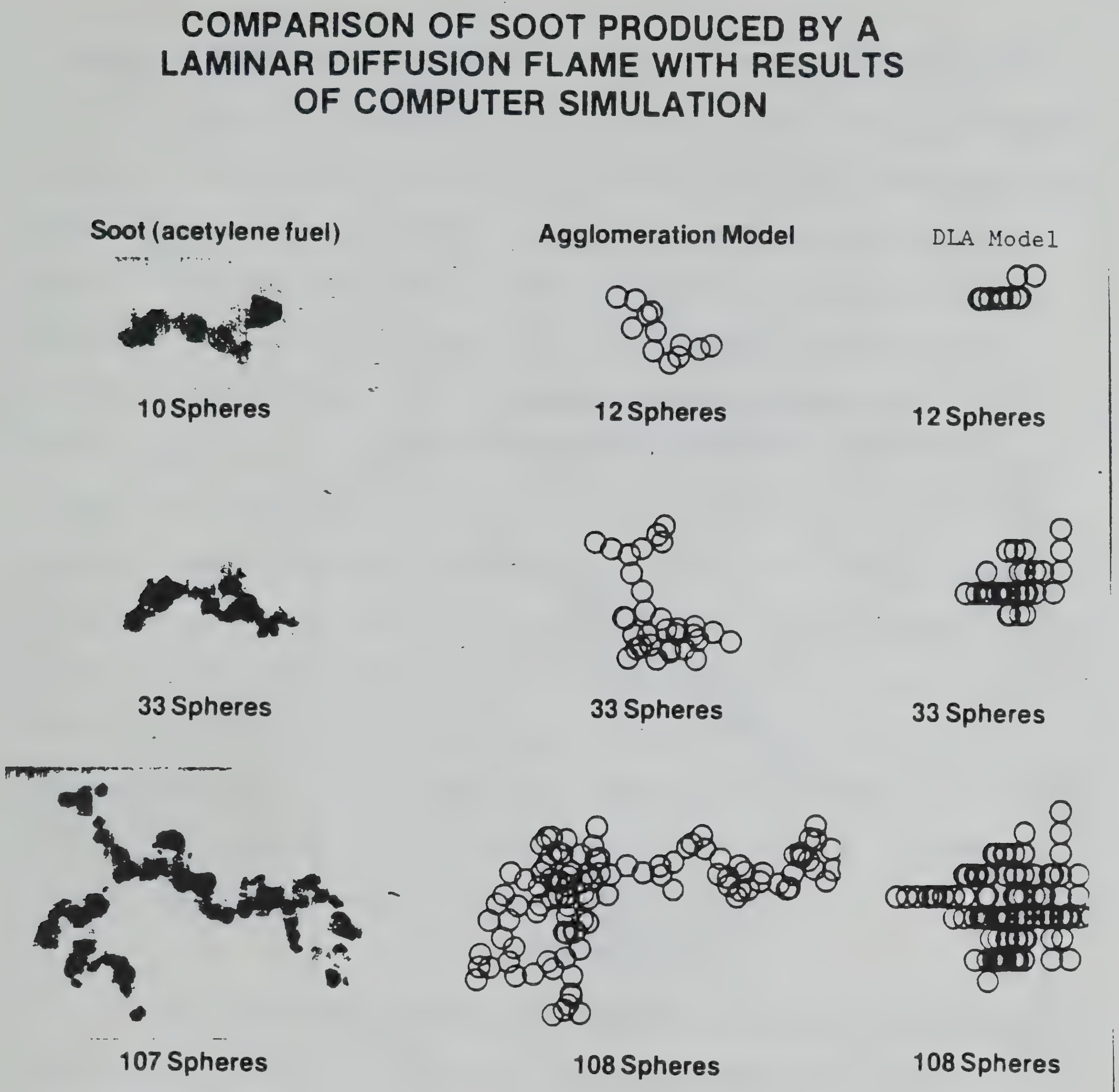

Figure 16. Qualitative comparison of clusters produced experimentally and by computer simulations.

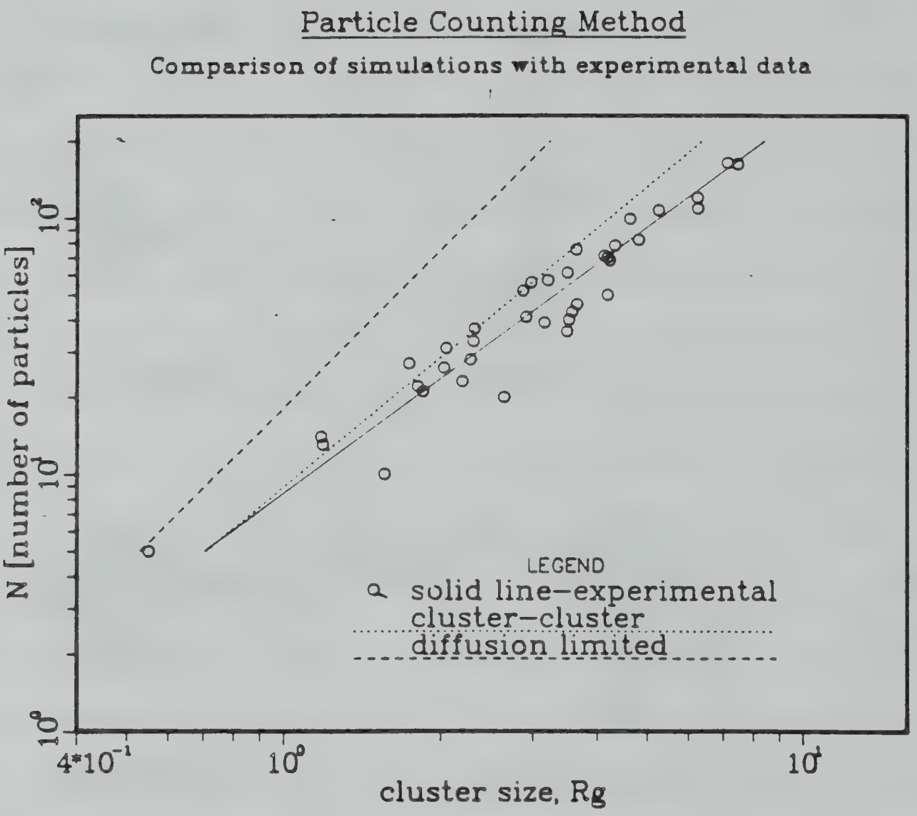

Particle Counting Method

Comparison of simulations with experimental data

Figure 17. R_g vs N plots of experimental and simulation data.

changes in growth mechanism occur for the extremely large clusters, or that they could not withstand external forces put upon them in the sample generation and preparation process. Assuming the growth process proceeds by some form of cluster-cluster agglomeration, single contact points which link clusters may not be sufficiently strong to maintain the agglomerate's overall structure. As a consequence, reshuffling of clusters to form denser, more stable agglomerates become likely during harsh collisions in backmixing or impaction on the TEM grid. To a lesser extent, dense structures can also arise from impaction of small clusters onto the sample immediately after it is collected, particularly those with a large surface area. Note the large number of clusters surrounding cluster number 2506 in figure 12b. Due to execution time restrictions, starting concentrations > 8,000 particles has yet to be performed for Mountain and Mulholland's simulation. Meakin[1984], reports $D_f \sim 1.80$ for clusters made up of 30,000 particles with the Monte-Carlo cluster-cluster agglomeration model.

We now compare our results to experimental values reported in the literature. Forrest and Witten[1979] produced Fe and Zn agglomerates by vaporization from an eletroplated tungsten filament. From pair correlation analyses of TEM images, the agglomerates were determined to have a $D_f \sim 1.5\text{-}1.7$. It was reported, however, that the agglomerates were not examined in their entirety. The extreme sizes allowed only a fraction of the total area of the agglomerate to be photographed. In any event, their pioneering work provided preliminary evidence of the fractal nature of these agglomerates.

Weitz and Huang[1985] presented an in-depth study of the kinetics and morphology of gold colloid agglomerates in aqueous solutions. Negatively charged gold spheres (d_p~14.5nm) which resist agglomeration due to repulsive forces were produced by the reduction of gold salt $Na(AuCl_4)$ with sodium nitrate. The addition of pyridine neutralizes the particles which then allow agglomeration to proceed. It was noted that the process is highly irreversible, owing to their ability to withstand physical or chemical separation measures. The agglomerates were found to have a dimensionality of 1.70 ± 0.1 from structural analysis of TEM projections by k versus $(LW)^{1/2}$ and c(r) versus r plots. As with the metal smokes of Forrest and Witten, no apparent change in D_f for small clusters were reported. The study however, satisfyingly showed that D_f is indeed invariant upon projection through confirmation of their results with small angle neutron scattering measurements in three dimensions.

In summary, experimental values of D_f ~1.80 for soot agglomerates ranging from 5-15 μm were found to be in agreement with Brownian motion simulations of cluster-cluster agglomeration using Monte-Carlo and Langevin trajectory approaches. There are obvious differences in results for small clusters (2-200 particles) and extremely large clusters (> 12 μm). This should not imply that the methods of analysis or the simulations are totally inadequate. We believe that some physical effects are responsible for the transition from D_f~1.5 to 1.9. Simulations currently take into account only a few of the controlling factors in a real system, and future work in this area should emphasize possible rearrangements due to weak bonding resulting from single contact points and more accurate simulations of the contributions of rotational motion. Conversely, experimental methods involving agglomeration at high temperature must be improved to minimize or eliminate effects of backmixing and grid impaction, and results should be verified by light scattering measurements. Experimental results suggest that fractal growth and structure are experienced by many agglomeration processes governed by the Brownian motion of particles and clusters. It is unlikely that D_f is a universal constant, but that differences in the environment (e.g. T, P, particle size and concentration) play an important role in cluster growth and structure.

VIII. Recommendations

The objective of this study was to characterize the structure of soot agglomerates in terms of the fractal dimension D_f from two dimensional projections of three-dimensional shapes. It is important that our findings be verified by methods that enable measurements in three dimensions. A promising approach is the reconstruction of the 3-D structure given projections at several tilt angles. At least two reference points, perhaps in the form of surrounding clusters are necessary to insure the proper accounting of particles. Another method is to measure the structure factor S(q) for scattering which, from a fractal, is expected to behave as

$$S(q) \sim q^{-D_f} \tag{11}$$

over some range of the momentum transfer q [Weitz and Huang,1984].

This study can also be extended to the examination of the relationships between the geometric size (R_g or $LW^{1/2}$) and shape L/W to other measurable properties such as aerodynamic diameters and diffusion constants. In the latter case, the applicability of the Stokes-Einstein relation

$$D = kT/f \tag{26}$$

where D = diffusion constant

k = Boltzmann's constant

T = absolute temperature

f = friction force, equal to $3\pi\mu d_p$ in the continuum regime, where μ is the gas viscosity and d_p is the particle diameter.

to agglomeration systems can be investigated by expressing d_p in terms of R_g or, in terms of the fractal relation

$$d_p \propto R_g \propto N^{1/D_f} \tag{27}$$

where N is the number of primary particles in the cluster.

IX. Literature Cited

1. Andersen 2000 ,Inc., "Operating Manual for Andersen 2000 Inc. 1.0ACFM Ambient Particle Sizing Samplers", Atlanta, GA., 1977.
2. Davies, C. N., "Aerosol Science", Academic Press, New York, N.Y., 1966.
3. Feder, J., Jossang, T., and Rosenquist, E., Physical Review Letters, 53, 1403, 1984.
4. Friedlander, S.K., "Smoke, Dust and Haze", John Wiley and Sons, New York, N.Y., 1977.
5. Forrest, S.R., and Witten, T.A., J. Physics A, 12, n5, 1979.
6. Gray, R.H., Kanapilly, G.M., Cheng, Y.S., and Wolff, R.K., J. Aerosol Science, 16, n3, 211, 1985.
7. Hausdorff, F., Math. Annal., 79, 157, 1919.
8. Hinds, W.C., "Aerosol Technology", John Wiley and Sons, New York, N.Y., 1982.
9. Kirkwood, J.G., and Mayer, J.E., "Phase Transformations in Solids", Wiley, New York, N.Y., 1951. edited by R. Smoluchowski.
10. Mandelbrot, B.B., "Fractals- Form, Chance, and Dimension", W.H. Freeman & Co., New York, N.Y., 1977.
11. Mandelbrot, B.B., "The Fractal Geometry of Nature", W.H. Freeman & Co., New York, N.Y., 1983.
12. Meakin, P., Physical Review A, 27, n1, 604, 1983.
13. Meakin, P., J. Colloid and Interface Science, 102, n2, 491, 1984.
14. Medalia, A.I., and Heckman, F.A., Journal of Colloid and Interface Science, 24, n2, 393, 1967.

15. Medalia, A.I., and Heckman, F.A., Journal of Colloid and Interface Science, 36, n2, 173, 1971.

16. Mountain, R.D., Mulholland, G.W., and Baum, H., to be published.

17. Santoro, R.J., Semerjian, H.G., and Dobbins, P.A., Combustion and Flame, 51, 203, 1983.

18. Siegla, Donald C., and Smith, George W., "Particulate Carbon Formation During Combustion", Plenum Press, New York, N.Y., 1981.

19. Sinha, S.K., Freltoft, T., and Kjems, J., "Kinetics of Aggregation and Gelation - Observation of Power Law Correlations in Silica-particle Aggregates by Small Angle Neutron Scattering", Elsevier Science Publishers, New York, N.Y., 1984. edited by F. Family and D.P. Landau.

20. Stanley, H.E., "Introduction to Phase Transitions and Critical Phenomena", Oxford University Press, New York, N.Y., 1971.

21. Sullivan, F. ,National Bureau of Standards, Gaithersburg, MD., private communication.

22. Smoluchowschi, M., Phys. Z., 17, 557, 1919.

23. Sutherland, D.N., and Goodarz-Nia, I., Chemical Engineering Science, 26, 2071, 1971.

24. Vold, M.J., Journal of Colloid Science, 18, 684, 1963.

25. Weitz, D.A., and Huang, J.S., "Kinetics of Aggregation and Gelation - Self similar structures in the Kinetics of Aggegation of Gold Colloids", Elsevier Science Publishers, pp 19-28, 1984. edited by F. Family and D.P. Landau.

26. Weitz, D.A., Huang, J.S., Lin, M.Y., and Sung, J., Physical Review Letters, 53, n17, 1657, 1984.

27. Witten, T.A., and Sander, L.M., Physical Review Letters, 47, 1400,1981.

28. Witten, T.A., and Sander, L.M., Physical review B, 27, n9, 5686, 1983.

X. Appendices

A. Successive Squares Method Program

```
      PROGRAM NEST
C
C
C     THIS PROGRAM USES THE SUCCESSIVE SQUARES METHOD WHICH
C     OUTPUTS N VS L(LENTH OF SIDE).
C     A SERIES OF CONCENTRIC SQUARES OF SIDE L ARE GENERATED
C     ABOUT THE CENTER OF MASS AND THE NUMBER OF OCCUPIED
C     SITES WITHIN EACH SQUARE IS COUNTED.
C
C
C     DEFINITION OF VARIABLES
C
C
C       PIXD(X,Y)= 512X512 MATRIX CONTAINING 1'S(OCCUPIED)
C                  AND 0'S(UNOCCUPIED).
C       CX,CY = CENTER OF MASS IN TWO DIMENSIONS
C       XX,YY = SUM OF ALL VALUES OF X,Y COORDINATES
C       LS = LENGTH OF SIDE
C
C
      INTEGER PIXD(512,512),COUNT,DX,DY,CX,CY,SIDE,LS,HS
      REAL XX,YY
      OPEN(1,FILE='INPUT')
      OPEN(2,FILE='OUTPUT')
C
C
C     ******* ZERO PIXD ARRAY *******
C
C
      DO 10 I=1,512
           DO 20 J=1,512
                PIXD(I,J)=0
20         CONTINUE
10    CONTINUE
C
C     ******* READ DATA AND COMPUTE CENTER OF MASS TO NEAREST INTEGER
C
      XX=0
      YY=0
      READ(1,*) NP
      DO 30 I=1,NP
           READ(1,*) DX,DY
           PIXD(DX,DY)=1
           XX=XX+DX*1.0
           YY=YY+DY*1.0
```

```
 30    CONTINUE
            XX=XX/(NP*1.0)
            YY=YY/(NP*1.0)
       CX=INT(XX+.5)
       CY=INT(YY+.5)
 C
 C
 C     ******* MAIN LOOP *******

C
C
      COUNT=0
      IF(PIXD(CX,CY).EQ.1) COUNT=1
      LS=400
      HS=LS/2
      DO 40 I=1,HS
           DO 50 K=-I,I,1
                IF (PIXD(CX+K,CY+I).EQ.1) COUNT=COUNT+1
50         CONTINUE
           DO 60 K=-I,I-1,1
                IF (PIXD(CX+I,CY+K).EQ.1) COUNT=COUNT+1
60         CONTINUE
           DO 70 K=-I.I-1,1
                IF (PIXD(CX+K,CY-I).EQ.1) COUNT=COUNT+1
70         CONTINUE
           DO 80 K=-I+1,I-1,1
                IF (PIXD(CX-I,CY+K).EQ.1) COUNT=COUNT+1
80         CONTINUE
           SIDE=I*2+1
           WRITE(2,*) SIDE.COUNT
40    CONTINUE
C
C
C     ******* FINISH NESTED SQUARES PROCEDURE *******
C
C
      STOP
      END
```

B. Pair Correlation Method Program

```
      PROGRAM PAIRCO
C
C       PROGRAM TO COMPUTE C(R) USING MOUNTAIN'S METHOD
C       READS IN 2-D SIMULATION OR EXPERIMENTAL DATA
C       LENGTH BETWEEN ANY TWO PARTICLES ARE COUNTED ONLY ONCE.
C
C
C      DEFINITION OF VARIABLES
C
C        DIST = DISTANCE BETWEEN TWO PARTICLES OR OCCUPIED SITES
C        LSQR = DIST**2
C        N(I) = NUMBER OF TIMES THE INTEGER DISTANCE I OCCURED
C               BETWEEN ALL OCCUPIED SITES.
C        PCORR = ACTUAL VALUE OF THE PAIR CORRELATION FUNCTION
C                OBTAINED FROM THE FOLLOWING EQUATION :
C
C                PCORR = (2.0*N(I))/(NP*MAX(I))
C
C        NP = TOTAL NUMBER OF OCCUPIED SITES
C        MAX(I) = TOTAL NUMBER OF POINTS IN A SHELL OF INNER
C                 RADIUS I-.5 AND OUTER RADIUS I+.5 IN A SQUARE
C                 LATTICE.
C        X() = ARRAY OF X COORDINATES
C        Y() = ARRAY OF Y COORDINATES
C
C
      REAL X(156000),Y(156000),DIST,LSQR,PAIRCO
      INTEGER N(1000),LENGTH
C
C
C       ******* OPEN STATEMENTS *******
C
C
      OPEN(UNIT=3,FILE='INPUT')
      OPEN(UNIT=4,FILE='OUTPUT')
C
```

```
C
C        ******* ZERO LENGTH ARRAY *******
C
C
         DO 10 I=1,1000
             N(I)=0
 10      CONTINUE
C
C
C        ******* READ DATA FROM FILE. *******
C
C
         READ(3,*) NN
         DO 20 I=1,NN
             READ(3,*) X(I),Y(I)
 20      CONTINUE
C



C
C        ******* BEGIN NESTED LOOP TO COMPUTE N(I)'S *******
C
C
         DO 30 I=1,NN-1
                 DO 40 J=I+1,NN
                     LSQR=(X(J)-X(I))**2 +(Y(J)-Y(I))**2
                     DIST=LSQR**.5
                     LENGTH=INT(DIST+.5)
                     N(LENGTH)=N(LENGTH)+1
 40              CONTINUE
 30      CONTINUE
C
C
C        ******* OUTPUT OF RESULTS *******
C
C
         DO 50 I=1,400
             IF (N(I).GT.0) WRITE(4,*) I,N(I)
 50      CONTINUE
C
C
C        ******* END OUTPUT *******
C
C
         STOP
         END
```

```
C
C
      PROGRAM NMALIZ2
C
C
C     THIS PROGRAM COMPUTES C(R) FROM THE N(I)'S GIVEN
C     BY PROGRAM PAIRCO.  THE MAXIMUM NUMBER OF OCCUPIED SITES
C     FOR EACH VALUE OF R IS STORED IN FILE 'DATMX2D' IN 2-D
C     UP TO R=250 AND 'DATMX3D' IN 3-D UP TO R=30.
C
C
      REAL MAX(250)
      INTEGER I,J,DUMMY
      CHARACTER IN*7,OUT*7
C
C
C     ******* OPEN STATEMENTS *******
C
C
      PRINT*,'ENTER INPUT FILE,OUTPUT FILE (APOSTROPHES NEEDED):'
      READ*,IN,OUT
      PRINT*,' ENTER NP: THE NUMBER OF OCCUPIED SITES'
      READ*,NP
C
C
C     ******* OPEN STATEMENTS *******
C
C
      OPEN(1,FILE=IN)
      OPEN(6,FILE=OUT)
      OPEN(2,FILE='DATMX2D')
C
C
      DO 10 I=1,250
          READ(2,*) J,DUMMY
          MAX(J)=DUMMY*1.0
10    CONTINUE
C
C
C      ******* NORMALIZE PAIRCO ******
C
C
      DO 20 I=1,250
          READ(1,*) J,PCORR
          PCORR= PCORR*2.0*(I*1.0)/((NP*1.0)*MAX(I))
          WRITE(6,*) I,PCORR
20    CONTINUE
      STOP
      END
```

C. Diffusion Limited Aggregation Program

```
       PROGRAM MK855
C
C
C      PROGRAM TO SIMULATE DIFFUSION LIMITED AGGREGATION IN
C      THREE DIMENSIONS.
C
C
C      DEFINITION OF VARIABLES
C
C
C         X(),Y(),Z() = 3-D COORDINATES OF PARTICLES BELONGING
C                       TO THE CLUSTER.
C         STP = DISTANCE IN LATTICE SPACINGS TRAVELED BY THE
C               PARTICLE PER STEP
C        DX,DY,DZ = CURRENT LOCATION OF DIFFUSING PARTICLE
C        RMAX = DISTANCE FROM THE ORIGIN TO THE FARTHEST
C               PARTICLE IN THE CLUSTER.
C        RSTART = RMAX+5, RADIUS ALONG WHICH PARTICLE BEGINS
C                 TO DIFFUSE
C        KILL = 2.0*RSTART, DISTANCE BEYOND WHICH PARTICLE IS
C               DESTROYED.
C        DISTCHK = DISTANCE BETWEEN TWO PARTICLES TO CHECK FOR
C                  COLLISION.
C        PHI,THETA = SPECIFIES SPHERICAL COORDINATES OF DIFFUSING
C                    PARTICLE STARTING POINT ALONG WITH RSTART
C        DIRECT = SPECIFIES DIRECTION RANDOMLY (6 POSSIBLE)
C
C
       INTEGER X(10000),Y(10000),Z(10000),STP,DX,DY,DZ,DIRECT
       REAL RMAX,DUMMY,RSTART,KILL,DIST,DISTCHK
C
C
C      OPEN STATEMENT FOR OUTPUT
C
C
       OPEN(UNIT=2,FILE='OUTPUT')
C
C
C      RANDOM NUMBER GENERATOR SEED= ISEED
C
C
       Z=1005
       CALL RANSET(Z)
```

```
C
C
C       INITIALIZE SEED COORDINATES
C
C
        X(1)=0
        Y(1)=0
        Z(1)=0
        WRITE(2,*) X(1),Y(1),Z(1)
        RMAX=0


C
C
C       BEGIN LOOP FOR DIFFUSION LIMITED AGGREGATION
C
C
        DO 10 I=2,5000
        DDX=X(I-1)*1.0
        DDY=Y(I-1)*1.0
        DDZ=Z(I-1)*1.0
        DUMMY = (DDX**2+DDY**2+DDZ**2)**.5
        IF(DUMMY.GT.RMAX) RMAX=DUMMY
        RSTART = RMAX+5.0
C
C
C ******* CHANGED KILL FROM 2*RSTART TO 1.5*RSTART *******
C
C
        KILL = 2.0*RSTART
 300    CONTINUE
C
C
C       RANDOM NUMBER FOR THETA AND PHI - SPHERICAL COORDINATES
C
C
        THETA=RANF()*3.141592654
        PHI=RANF()*2.0*3.141592654
        DX = INT(RSTART*SIN(THETA)*COS(PHI))
        DY = INT(RSTART*SIN(THETA)*SIN(PHI))
        DZ = INT(RSTART*COS(THETA))
 400    CONTINUE
        STP = 1
        DIST = (DX**2+DY**2+DZ**2)**.5
C
C
C       CHANGE STEPSIZE AS THE PARTICLE WALKS IN DIRECTION AWAY
C       FROM CLUSTER.
C
C
```

```
      IF(DIST.LE.RMAX+10) GOTO 200
      IF(DIST.GT.RMAX+10) STP=2
      IF(DIST.GT.RMAX+20) STP=4
      IF(DIST.GT.RMAX+40) STP=8
      IF(DIST.GT.RMAX+80) STP=16
 200  CONTINUE
      DIRECT=INT(6*RANF()+1)
C
C
C     CHOOSE DIRECTION OF WALK RANDOMLY - 6 POSSIBLE DIRECTIONS
C
C
      IF(DIRECT.EQ.1) DX=DX-STP
      IF(DIRECT.EQ.2) DX=DX+STP
      IF(DIRECT.EQ.3) DY=DY-STP



      IF(DIRECT.EQ.4) DY=DY+STP
      IF(DIRECT.EQ.5) DZ=DZ-STP
      IF(DIRECT.EQ.6) DZ=DZ+STP
      DIST=(DX**2+DY**2+DZ**2)**.5
      IF(DIST.GT.KILL) GOTO 300
      IF(DIST.GT.RMAX+2) GOTO 400
C
C
C     DETERMINE WHETHER A HIT OCCURS.
C     HIT IF DISTANCE TO ANY PARTICLE IN CLUSTER = 1.
C
C
      DO 20 J=1,I-1
          DISTCHK=(X(J)-DX)**2 + (Y(J)-DY)**2 + (Z(J)-DZ)**2
          IF(DISTCHK.EQ.1) GOTO 40
 20   CONTINUE
C
C
C     REPEAT RANDOM WALK IF NO HIT. ELSE GO TO 40.
C
C
      GOTO 400
 40   CONTINUE
      X(I)=DX
      Y(I)=DY
      Z(I)=DZ
      WRITE(2,*) X(I),Y(I),Z(I)
 10   CONTINUE
C
C
C     END DLA LOOP.
C
C
      END
```

D. Monte-Carlo Digitization Program

```
      PROGRAM DIGITIZ
C
C     PROGRAM TO 'DIGITIZE' THE CLUSTER GENERATED FROM MOUNTAIN'S
C     PROGRAM TO SIMULATE THE ACTUAL DIGITIZATION PROCESS. RESULTS
C     WILL BE USED TO EVALUATE THE PAIR CORRELATION FUNCTION.
C
      REAL X(9999),Y(9999),Z(9999)
      OPEN(UNIT=1,FILE='INPUT')
      OPEN(UNIT=2,FILE='OUTPUT')
      Z=1931
      CALL RANSET(Z)
C
C     READ COORDINATES FROM FILE
C
      READ(1,*) NP
      DO 10 I=1,NP
          READ(1,*) Z(I),X(I),Y(I)
10    CONTINUE
C
C
C     BEGIN MONTE-CARLO INTEGRATION PROCEDURE
C
C
C     FOR FILE DATAABQ,   XMIN=11    XMAX= 59
C                         YMIN=-49   YMAX=18.2
C                         ZMIN=-4    ZMAX=47
C
      DO 20 I=-50,20
      DO 30 J=-5,49
            COUNT=0
            DO 40 K=1,100
                  RANX=RANF()-0.5
                  RANY=RANF()-0.5
                  TX=(I*1.0)+RANX
                  TY=(J*1.0)+RANY
                  DO 50 L=1,NP
                        DIST=((TX-X(L))**2+(TY-Y(L))**2)**.5
                        IF(DIST.LE.0.5) THEN
                             COUNT=COUNT+1
                             GOTO 60
                        END IF
50                CONTINUE
60                CONTINUE
                  IF(COUNT.GT.50) THEN
                             WRITE(2,*) I,J
                             GOTO 70
                  END IF
40          CONTINUE
70          CONTINUE
30    CONTINUE
20    CONTINUE
      STOP
      END
```

NBS-114A (REV. 2-80)

U.S. DEPT. OF COMM.

BIBLIOGRAPHIC DATA SHEET *(See instructions)*

1. PUBLICATION OR REPORT NO.
NBS/GCR-88-549

2. Performing Organ. Report No.

3. Publication Date
June 1988

4. TITLE AND SUBTITLE
Fractal Analysis of Soot Agglomerates

5. AUTHOR(S)
Roberto J. Samson

6. PERFORMING ORGANIZATION *(If joint or other than NBS, see instructions)*

University of Maryland
College Park, MD 20742

7. Contract/Grant No.
COM70NAN85H0517

8. Type of Report & Period Covered
Final Report
June 1986 - June 1987

9. SPONSORING ORGANIZATION NAME AND COMPLETE ADDRESS *(Street, City, State, ZIP)*

National Bureau of Standards
U.S. Department of Commerce
Gaithersburg, MD 20899

10. SUPPLEMENTARY NOTES

☐ Document describes a computer program; SF-185, FIPS Software Summary, is attached.

11. ABSTRACT *(A 200-word or less factual summary of most significant information. If document includes a significant bibliography or literature survey, mention it here)*

The fractal behavior of soot agglomerates formed by the combustion of acetylene in a coannular diffusion burner is studied. Structural data from electron micrographs were obtained by two methods: the first by particle counting with the aid of stereopairs for small clusters, and the second by electronic digitization with advanced image processing techniques, used for the larger agglomerates. An average agglomerate length to width ratio of about 1.7 with a standard deviation of 0.6 was obtained. The agglomerates were found to have a fractal dimension D_f of about 1.8-1.9 based on measurements of the pair correlation function for large agglomerates and 1.5-1.6 based on measurements of the radius of gyration for small agglomerates. These results are compared with recent computer simulations as well as experimental studies of inorganic smokes.

This work performed on Grant No. COM-70-NAN85H0517. Kinetics of Aggregate Formation, Principal Investigator: James W. Gentry.

12. KEY WORDS *(Six to twelve entries; alphabetical order; capitalize only proper names; and separate key words by semicolons)*

acetylene; agglomerates; data analysis; simulation; smoke; soot

13. AVAILABILITY

☒ Unlimited

☐ For Official Distribution. Do Not Release to NTIS

☐ Order From Superintendent of Documents, U.S. Government Printing Office, Washington, D.C. 20402.

☒ Order From National Technical Information Service (NTIS), Springfield, VA. 22161

14. NO. OF PRINTED PAGES
94

15. Price
$13.95

USCOMM-DC 6043-P80